

OCT 20 2004

REPORT DOCUMENTATION PAGE			Form Approved OMB No. 0704-0188	
Public reporting burden for this collection of information is estimated to average 1 hour per response, including the time for reviewing instructions, searching existing data sources, gathering and maintaining the data needed, and completing and reviewing the collection of information. Send comments regarding this burden estimate or any other aspect of this collection of information, including suggestions for reducing this burden, to Washington Headquarters Services, Directorate for Information Operations and Reports, 1215 Jefferson Davis Highway, Suite 1204, Arlington, VA 22202-4302, and to the Office of Management and Budget, Paperwork Reduction Project (0704-0188), Washington, DC 20503.				
1. AGENCY USE ONLY (Leave blank)	2. REPORT DATE 19.Oct.04	3. REPORT TYPE AND DATES COVERED THESIS		
4. TITLE AND SUBTITLE SMALL FIELD DOSIMETRY COMPARING MEASURED DATA VERSUS THE ADAC PINNACLE 3 MODEL		5. FUNDING NUMBERS		
6. AUTHOR(S) CAPT LUDOLPH DANIEL A				
7. PERFORMING ORGANIZATION NAME(S) AND ADDRESS(ES) UNIVERSITY OF TEXAS HSC AT SAN ANTONIO		8. PERFORMING ORGANIZATION REPORT NUMBER CI04-648		
9. SPONSORING/MONITORING AGENCY NAME(S) AND ADDRESS(ES) THE DEPARTMENT OF THE AIR FORCE AFIT/CIA, BLDG 125 2950 P STREET WPAFB OH 45433		10. SPONSORING/MONITORING AGENCY REPORT NUMBER		
11. SUPPLEMENTARY NOTES				
12a. DISTRIBUTION AVAILABILITY STATEMENT Unlimited distribution In Accordance With AFI 35-205/AFIT Sup 1		12b. DISTRIBUTION CODE DISTRIBUTION STATEMENT A Approved for Public Release Distribution Unlimited		
13. ABSTRACT (Maximum 200 words)				
20041025 009				
14. SUBJECT TERMS		15. NUMBER OF PAGES 76		
		16. PRICE CODE		
17. SECURITY CLASSIFICATION OF REPORT	18. SECURITY CLASSIFICATION OF THIS PAGE	19. SECURITY CLASSIFICATION OF ABSTRACT	20. LIMITATION OF ABSTRACT	

BEST AVAILABLE COPY

Standard Form 298 (Rev. 2-89) (EG)
Prescribed by ANSI Std. Z39.18
Designed using Perform Pro, WHS/DIOR, Oct 94

**SMALL FIELD DOSIMETRY COMPARING MEASURED DATA VERSUS THE
ADAC PINNACLE 3 MODEL**

A THESIS

Presented to the Faculty of

The University of Texas Health Science Center at San Antonio

Graduate School of Biomedical Sciences

in Partial Fulfilment

of the Requirements

for the Degree of

MASTER OF SCIENCE IN MEDICAL PHYSICS

BY

DANIEL ANTHONY LUDOLPH, B.S., M.S.

SAN ANTONIO, TX

AUGUST 2004

DISTRIBUTION STATEMENT A
Approved for Public Release
Distribution Unlimited

*This thesis is dedicated with love to my wife, [REDACTED], for her never ending
support in my endeavors.*

I would like to take this opportunity to thank my committee members; Dr. Bill Bice, Dr. Wang, Dr. Blough, and Dr. Hussey, for their support in my research and thesis. I would like to further extend my gratitude to my good friend Dr. Paul Hanny. Although not a committee member, he was instrumental in this endeavor. Lastly I would like to express my appreciation to Dr. Donald Dubois for mentoring me as I navigate the career field of a Medical Physicist.

**SMALL FIELD DOSIMETRY COMPARING MEASURED DATA VERSUS THE
ADAC PINNACLE 3 MODEL**

Publication No. _____

Daniel Anthony Ludolph, M.S.

The University of Texas Health Science Center at San Antonio

Graduate School of Biomedical Sciences

Supervising Professor: William Bice, S., PhD.

Intensity Modulated Radiation Therapy (IMRT) is rapidly becoming the standard of care for external radiation beam therapy. With IMRT, the radiation beam is effectively broken up into thousands of tiny pencil-thin radiation beams. High speed computers employing complex dose algorithms have the ability to plan and predict doses for IMRT treatment plans. While this method can optimize conformity to tumors and provide better sparing of surrounding tissue, it also presents a host of challenges due to reliance on dosimetry data for small field sizes. Small field dosimetry in itself is a challenge. There many factors that can influence the accuracy of the data. Despite these obstacles it is imperative that accurate data be used in treatment

planning systems to provide the best optimized plans. The objective of this work was to test whether ADAC Pinnacle 3 can accurately predict doses for small field sizes. Small field profile data using jaw and multileaf collimation was collected using Kodak EDR2 film. The measured profiles were then compared to the ADAC predicted profiles. The measured data was used to construct small field models for both jaw and multileaf collimation. Using views from actual IMRT plans, the measured models were then compared to the ADAC model.

**SMALL FIELD DOSIMETRY COMPARING MEASURED DATA VERSUS THE
ADAC PINNACLE 3 MODEL**

Publication No. _____

Daniel Anthony Ludolph, M.S.

The University of Texas Health Science Center at San Antonio

Graduate School of Biomedical Sciences

Supervising Professor: William Bice, S., PhD.

Intensity Modulated Radiation Therapy (IMRT) is rapidly becoming the standard of care for external radiation beam therapy. With IMRT, the radiation beam is effectively broken up into thousands of tiny pencil-thin radiation beams. High speed computers employing complex dose algorithms have the ability to plan and predict doses for IMRT treatment plans. While this method can optimize conformity to tumors and provide better sparing of surrounding tissue, it also presents a host of challenges due to reliance on dosimetry data for small field sizes. Small field dosimetry in itself is a challenge. There many factors that can influence the accuracy of the data. Despite these obstacles it is imperative that accurate data be used in treatment

planning systems to provide the best optimized plans. The objective of this work was to test whether ADAC Pinnacle 3 can accurately predict doses for small field sizes. Small field profile data using jaw and multileaf collimation was collected using Kodak EDR2 film. The measured profiles were then compared to the ADAC predicted profiles. The measured data was used to construct small field models for both jaw and multileaf collimation. Using views from actual IMRT plans, the measured models were then compared to the ADAC model.

**THE VIEWS EXPRESSED IN THIS ARTICLE ARE
THOSE OF THE AUTHOR AND DO NOT REFLECT
THE OFFICIAL POLICY OR POSITION OF THE
UNITED STATES AIR FORCE, DEPARTMENT OF
DEFENSE, OR THE U.S. GOVERNMENT.**

TABLE OF CONTENTS

	Page
Title.....	i
Approval.....	ii
Dedication.....	iii
Acknowledgements.....	iv
Abstract.....	v
Table of contents.....	vii
List of figures.....	ix
I. INTRODUCTION.....	1
II. MATERIALS AND METHODS.....	4
III. RESULTS.....	9
A. Jaw Profiles.....	9
B. MLC Profiles.....	17
C. Head and Neck planar dose Data and Images.....	25
1. Comparison of planar Images.....	25
2. Comparison of calculated deliverable Data.....	28
3. Comparison of calculated deliverable vs. deliverable measured Data.....	32

D. Prostate planar dose Data and Images.....	46
1. Comparison of planar Images.....	46
2. Comparison of calculated deliverable Data.....	49
3. Comparison of calculated deliverable vs. deliverable measured Data.....	53
IV. DISCUSSION.....	67
V. CONCLUSIONS.....	69
APPENDIX.....	70
LITERATURE CITED.....	76
VITA.....	77

LIST OF FIGURES

	Page
Figure 1	Beam Profile, Jaw vs. ADAC, 1cm ²10
Figure 2	Beam Profile, Jaw vs. ADAC, 2cm ²11
Figure 3	Beam Profile, Jaw vs. ADAC, 3cm ²12
Figure 4	Beam Profile, Jaw vs. ADAC, 4cm ²13
Figure 5	Beam Profile, Jaw vs. ADAC, 5cm ²14
Figure 6	Depth dose Profile, Jaw vs. ADAC, 2cm ²15
Figure 7	Depth dose Profile, Jaw vs. ADAC, 5cm ²16
Figure 8	Beam Profile, MLC vs. ADAC, 1cm ²18
Figure 9	Beam Profile, MLC vs. ADAC, 2cm ²19
Figure 10	Beam Profile, MLC vs. ADAC, 3cm ²20
Figure 11	Beam Profile, MLC vs. ADAC, 4cm ²21
Figure 12	Beam Profile, MLC vs. ADAC, 5cm ²22
Figure 13	Depth dose Profile, MLC vs. ADAC, 2cm ²23
Figure 14	Depth dose Profile, MLC vs. ADAC, 5cm ²24
Figure 15	Planar dose Image, Head and Neck, ADAC Data.....26
Figure 16	Planar dose Image, Head and Neck, Jaw Data.....27
Figure 17	Planar dose Image, Head and Neck, MLC Data.....27
Figure 18	Vertical dose Profile Comparison, ADAC vs. Jaw.....29
Figure 19	Horizontal dose Profile Comparison, ADAC vs. Jaw.....29
Figure 20	Vertical dose Profile Comparison, ADAC vs. MLC.....30

LIST OF FIGURES (CON)

	Page
Figure 21	Horizontal dose Profile Comparison, ADAC vs. MLC.....30
Figure 22	Isodose Map Comparison, ADAC vs. Jaw.....31
Figure 23	Isodose Map Comparison, ADAC vs. MLC.....31
Figure 24	NAT Image, ADAC calculated vs. ADAC measured.....33
Figure 25	DTA Image, ADAC calculated vs. ADAC measured.....33
Figure 26	Isodose Map, ADAC calculated vs. ADAC measured.....34
Figure 27	Vertical dose Profile Comparison, ADAC vs. ADAC.....34
Figure 28	Horizontal dose Profile Comparison, ADAC vs. ADAC.....35
Figure 29	2D Dose/Distance Histogram, ADAC vs. ADAC.....35
Figure 30	NAT Image, MLC calculated vs. MLC measured.....37
Figure 31	DTA Image, MLC calculated vs. MLC measured.....37
Figure 32	Isodose Map, MLC calculated vs. MLC measured.....38
Figure 33	Vertical dose Profile Comparison, MLC vs. MLC.....38
Figure 34	Horizontal dose Profile Comparison, MLC vs. MLC.....39
Figure 35	2D Dose/Distance Histogram, MLC vs. MLC.....39
Figure 36	NAT Image, Jaw calculated vs. Jaw measured.....41
Figure 37	DTA Image, Jaw calculated vs. Jaw measured.....41
Figure 38	Isodose Map, Jaw calculated vs. Jaw measured.....42
Figure 39	Vertical dose Profile Comparison, Jaw vs. Jaw.....42

LIST OF FIGURES (CON)

	Page
Figure 40	Horizontal dose Profile Comparison, Jaw vs. Jaw.....43
Figure 41	2D Dose/Distance Histogram, Jaw vs. Jaw.....43
Figure 42	Table, Calculated deliverable vs. deliverable measured Data.....45
Figure 43	Planar dose Image, Prostate, ADAC Data.....47
Figure 44	Planar dose Image, Prostate, Jaw Data.....48
Figure 45	Planar dose Image, Prostate, MLC Data.....48
Figure 46	Vertical dose Profile, ADAC vs. Jaw Model.....50
Figure 47	Horizontal dose Profile, ADAC vs. Jaw Model.....50
Figure 48	Vertical dose Profile, ADAC vs. MLC Model.....51
Figure 49	Horizontal dose profile, ADAC vs. MLC Model.....51
Figure 50	Isodose Map, ADAC vs. Jaw Model.....52
Figure 51	Isodose Map, ADAC vs. MLC Model.....52
Figure 52	NAT Image, ADAC calculated vs. ADAC measured.....54
Figure 53	DTA Image, ADAC calculated vs. ADAC measured.....54
Figure 54	Isodose Map, ADAC calculated vs. ADAC measured.....55
Figure 55	Vertical dose Profile Comparison, ADAC vs. ADAC.....55
Figure 56	Horizontal dose Profile Comparison, ADAC vs. ADAC.....56
Figure 57	2D Dose/Distance Histogram, ADAC vs. ADAC.....56
Figure 58	NAT Image, MLC calculated vs. MLC measured.....58

LIST OF FIGURES (CON)

	Page
Figure 59	DTA Image, MLC calculated vs. MLC measured.....58
Figure 60	Isodose Map, MLC calculated vs. MLC measured.....59
Figure 61	Vertical dose Profile, MLC vs. MLC.....59
Figure 62	Horizontal dose Profile, MLC vs. MLC.....60
Figure 63	2D Dose/Distance Histogram, MLC vs. MLC.....60
Figure 64	NAT Image, Jaw calculated vs. Jaw measured.....62
Figure 65	DTA Image, Jaw calculated vs. Jaw measured.....62
Figure 66	Isodose Map, Jaw calculated vs. Jaw measured.....63
Figure 67	Vertical dose Profile, Jaw vs. Jaw.....63
Figure 68	Horizontal dose Profile, Jaw vs. Jaw.....64
Figure 69	2D Dose/Distance Histogram, Jaw vs. Jaw.....64
Figure 70	Table, Calculated deliverable vs. deliverable measured Data.....66

I. INTRODUCTION

Intensity Modulated Radiation Therapy (IMRT) is the most technologically advanced treatment method available in external beam radiation therapy. In recent years the advantages of IMRT have been well established and, not surprisingly, there has been increased reliance of IMRT accelerator-based radiation therapy versus 3D conformal treatment¹.

With IMRT, the radiation beam is effectively broken up into thousands of pencil-thin radiation beams. This approach takes advantage of steep dose gradients allowing for a more conformal treatment plan, which translates to improved sparing of normal tissue. A common technique of creating IMRT beams is to employ a segmentation algorithm, which then converts an ideal fluence map into deliverable beam segments. These pencil thin beams are formed by multileaf collimators (MLC's), which narrow down a larger beam into a series of small rectangular fields. These small rectangular fields are typically 1.0 cm² or larger. While this technology represents a vast improvement over typical external beam therapy, it also may present a host of potential problems when it comes to treatment planning.

During treatment using these MLC beams, the separation distance between the MLC's may be as little as 5 mm for delivery of IMRT. One of the challenges of this type of delivery is whether or not the treatment planning software, such as ADAC Pinnacle, can accurately model these small fields inherent to IMRT plans and provide accurate dosimetry data. Small field dosimetry in itself presents a challenge. Issues of penumbra, scatter, and volume effect can all adversely affect data. Add to this the anomalies

associated with MLC's i.e., interleaf leakage, intraleaf transmission, leaf-end transmission, and one begins to realize how daunting the dosimetric challenges can be.

Penumbra is the region at the edge of the beam over which the dose rate changes rapidly as a function of distance from the beam axis. In one study, Bayouth *et. al.*² determined the penumbra for 1cm² fields to be 0.36cm +/- 0.03cm for 99% of the measurements. Proper penumbra calculation is critical for IMRT treatment planning systems. The position of the MLC leaves depends on the penumbra calculated by the planning software. Inaccurate calculation of penumbra may result in cold or hot spots between two adjacent fields.

With regards to the detector size (volume effect) in the dosimetry of small fields, Laub *et.al.*³ determined that while using a 0.6 cm³ Farmer chamber, deviations between the absolute point dose values calculated in ADAC Pinnacle and dose values measured with the chamber were as high as 6%. With a pinpoint chamber, (e.g., PTW-Freiburg diode type), deviations were as low as 2%.

Bayouth *et.al.*⁴ concluded in their study that interleaf leakage ranged from 1.0%-1.5%, while intraleaf transmission and leaf-end transmission ranged from 0.6%-0.8% and 0.8%-2.7% respectively.

Modeling by treatment planning systems must be able to account for these inherent small field dosimetry issues. While there has been some work done to describe the large field size dosimetric characteristics of MLC's^{5,6,7}, there is still much to be studied in order to describe the small field dosimetric characteristics of MLC's and whether or not significant differences exist. The objective of this work was to investigate

whether or not a clinically significant difference exists in the measured dose when using the current ADAC Pinnacle³ IMRT model, which is based on large field size data, versus using a small field models, based on small field measurements.

II. MATERIALS AND METHODS

A. EXPOSURES

Our institution, Wilford Hall Medical Center, Lackland AFB, TX recently purchased a Varian (Varian Medical Systems, Palo Alto, CA) 21EX Linac with 120 leaf MLC IMRT capability. Each leaf and carriage was independently controlled. Leaf movement was in the "X" direction (parallel with the lower jaws). Maximum leaf retract position for the Linac 21EX is 20.1 cm from the beam centerline and maximum leaf extend position is -20.0 cm over the beam centerline. The leaf thickness is 5 mm; the leaf height is 60.0 mm with an end radius of 80.0 mm. The leaf tongue and groove offsets are 0.4 mm. The coincidence light field vs. x-ray is 1 mm. Penumbra is 20-80% leaf end; 7 mm or less for a 10cm x 10cm field for x-ray energies <10MV, and 8.5 mm or less for higher energies. The average leaf transmission is <2.5% and the maximum interleaf leakage is <4.0%.⁸

Small field dosimetry data was collected using Kodak EDR2 ReadyPak[®] film (Eastman Kodak Company, Rochester, NY). All exposures were made at 100cm SAD, 6MV, 300 monitor units (1 MU = 1cGy), at depths of 1.5 cm, 5.0 cm, 10 cm, 15cm, and 20 cm. Field sizes ranged from 5 cm² to 1 cm² reducing the field size by 1cm² increments. Two sets of exposures were made, one using primary jaws to collimate, the other using the MLC to collimate. The films were processed with a Kodak 5000 rapid film processor. A calibration film was taken in conjunction with the dosimetry films.

Film calibration was performed using the method presented by Hanny *et.al*⁹.

Once processed, films were then scanned using a VIDAR[®] DosimetryPRO™ Advantage Film Digitizer (Vidar Systems Corporation, Herndon, VA). This scanner uses 32-bit data path outputting to 16 bits of greyscale for high resolution. The scanned images were then captured, cropped, and saved with a 75 dots per inch (dpi) resolution. The net optical densities were plotted as a function of the measured dose to produce the sensitometric curve data. Data were then analyzed by a nonlinear least squares fit of the beam sensitometric curve data to the double-double hit film response model described by Zhu *et.al.*:¹⁰

$$OD = OD_{1,max} [1 - e^{-\alpha_1 D} (1 + \alpha_1 D)] + OD_{2,max} [1 - e^{-\alpha_2 D} (1 + \alpha_2 D)]$$

where the OD is the optical density of the EDR2 film, $OD_{1,max}$ and $OD_{2,max}$ are the maximum optical densities, α_1 and α_2 are coefficients related to film sensitivity (cGy^{-1}), and D is the delivered dose (cGy).

With optical densities converted to dose, beam profiles were then generated. For each profile it was assumed that median value of the dose values equal to or greater than 50% of the maximum dose represented the mid-point of the profile. This point was assigned an "X" value of zero and subsequent "X" positions were assigned using the distance between each dot to form the "X" axis of the profile. The data was then converted into ASCII format and imported into ADAC Pinnacle³.

Using this profile data, two separate models were created:

- 1.) **Jaw model**- Small field size model constructed with data from field sizes of 5 cm x 5 cm and smaller using primary jaw collimation

2.) **MLC model**- Small field size model constructed with data from field sizes of 5 cm x 5 cm and smaller using MLC collimation

A series of comparisons were made using Pinnacle³® IMRT treatment planning software to test the Jaw model, and MLC model, against the standard **ADAC model**. The ADAC model is based on large field size data, i.e., 5 cm x 5 cm and larger. Even though technically all three models were designed in ADAC Pinnacle, to avoid confusion they will be labeled this point forward as the Jaw, MLC, and ADAC models.

The following describes algorithm that ADAC Pinnacle³® IMRT treatment planning software uses. The Pinnacle³® Collapsed Cone Convolution Superposition dose algorithm is based on the work of Mackie, *et.al.*¹¹ Rather than correcting measured dose distributions, the Convolution Superposition algorithm computes dose distributions from first principles and, therefore, can account for the effects of beam modifiers, the external patient contour, and tissue heterogeneities on the dose distribution. The Convolution Superposition dose model consists of four parts:

- Modeling the incident energy fluence as it exits the accelerator head.
- Projection of this energy fluence through the density representation of a patient to compute a TERMA (Total Energy Released per unit Mass) volume.
- A three-dimensional superposition of the TERMA with an energy deposition kernel using a ray-tracing technique to incorporate the effects of heterogeneities on lateral scatter.
- Electron contamination is modeled with an exponential falloff which is added to the dose distribution after the photon dose is computed.⁹

The series of comparisons looked at how the Jaw and MLC models each compared to the ADAC model. The first test was to compare the lateral beam profiles, at a depth of 1.5 cm (dmax). The Jaw model profile was compared to the ADAC model and likewise the MLC model was compared to the ADAC model.

To provide further analysis of the three models, a single plane from two separate IMRT plans (a head and neck plan and a prostate plan) were used. For the head and neck IMRT plan the right lateral view was used to generate three separate planar dose profiles, each based on one of the three models (ADAC, MLC, Jaw). For the prostate IMRT plan the PA view was used to do the same.

Using ADAC Pinnacle SmartSim to determine the effect of the models on the conversion process, the calculated optimized plans were converted to calculated deliverable plans for each of the models. The calculation parameters used in ADAC were; Error tolerance 2%, Minimum segment area 2cm^2 , Minimum equivalent square 2cm, Leaf field edge overlap 0.5 cm. Planar dose images were then constructed to determine if any significant discrepancies were visually appreciated.

In order to compare the calculated deliverable plans for each of the models, the planar dose data was imported into Dose Lab software, Version 3.05. The Jaw and MLC models' calculated deliverable data was compared to the ADAC model calculated deliverable data using vertical and horizontal dose profiles, and isodose maps.

Using the planar dose data from each of the respective models and planes, MLC segment exposures were made using the same film and set up as the previous profile exposures. The films were processed, scanned, and sensitometric data determined. To determine how accurately each model predicted its' measured data, a comparison was

made between the calculated deliverable data and the deliverable measured data. Using Dose Lab software a NAT (Normalized Agreement Test) and DTA (distance to agreement) test were performed for each model.

DTA calculations are based on the number of contour lines assigned. For this project a total of 7 isodose lines were chosen (25cGy, 65cGy, 75cGy, 85cGy, 90cGy, 98cGy). Coordinates of isodose lines are generated for a particular dose level on both the measured and computed images. A point on the measured isodose line is chosen, and the distance from every computed isodose point to the measured point is calculated. The DTA image is assigned the value of the minimum distance found at the same coordinate as the point in the measured image. This is repeated for all of the measured isodose points and other isodose lines.

The NAT image is based on local percent difference and DTA values. If a pixel passes the percent difference or DTA criteria, its NAT value is zero. To make it more useful clinically, the NAT value is assigned zero for cold areas outside the PTV (defined as areas with computed doses less than 75% of the maximum dose as defined in the patient information) and the deviations from dose and distance criteria are scaled by dose. The NAT index is the average NAT value divided by the average value of the dose scaling matrix. This single number represents the overall goodness of the dose agreement (lower numbers are better).

Also compared were vertical and horizontal dose profiles, as well as isodose maps. For completeness a 2D histogram of the percent of pixels that had a 3% dose or a 3mm distance difference was generated. While it was helpful in determining dose and distance criteria, its loss of spatial information should be considered.

III. RESULTS

A. JAW PROFILES

The following figures (1-5) are lateral beam profiles generated by the measured data using jaws for collimation, and compared to the ADAC model. Figures 6 and 7 represent depth dose data comparisons for the 2 cm² and 5 cm² field sizes.

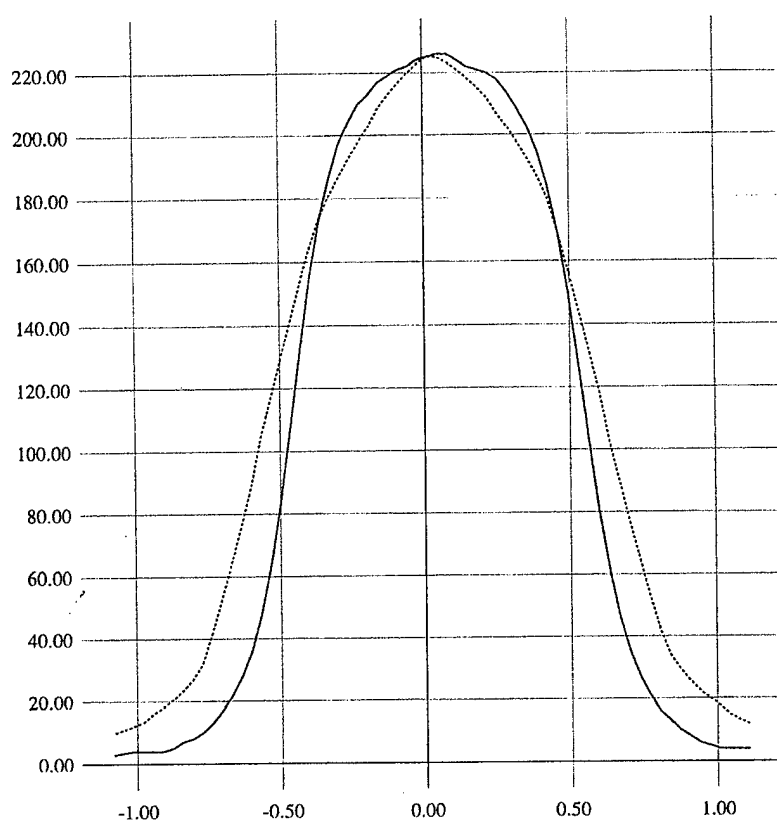
For the smaller field sizes, 1 cm² – 3 cm² the measured data from jaw collimation varied from ADAC by a range of 2% - 11%. For the 1 cm² profile the measured data reflected a higher dose in the central part of the field but a lower dose in the penumbra region. For the 2 cm² field size, there was good agreement in the central part of the profile with slight deviation at the edges. The 3 cm² profile reflected the greatest inconsistency the measured data reflecting a lower dose profile compared to the ADAC model. For the 4 cm² and 5 cm² field sizes, the measured profiles compared well with the ADAC model with differences \leq 2%. It was expected that for these larger field sizes, there would be good agreement. The differences seen with the smaller field sizes suggest that ADAC predicts a higher dose than was actually measured with film at the central 50% of the beam. The depth dose comparison shows good agreement between the Jaw and ADAC model.

Pinnacle³
Printed 07/21/04

Machine: Do not Use! (Jaw) Version: (uncommis
Energy: 6 MV Jaw
Geometry: SSD = 100 cm Field: 1 X 1

X: Depth= 1.50

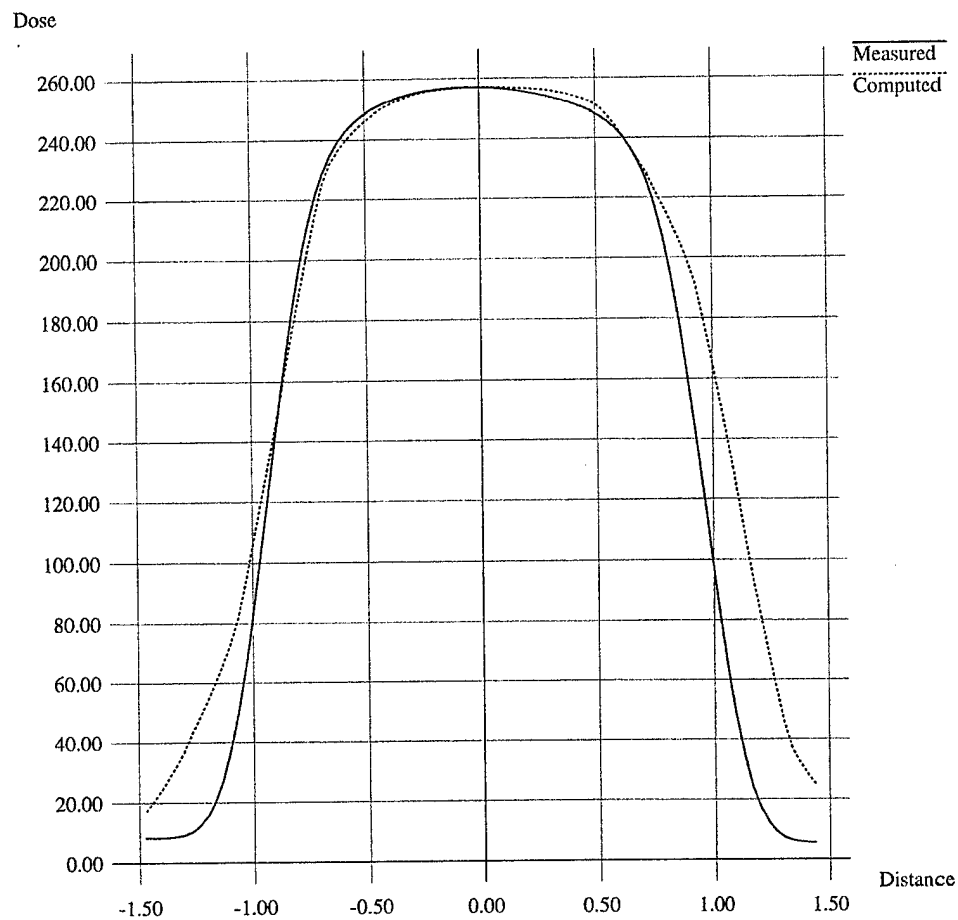
Dose



Pinnacle³
Printed 07/07/04

Machine: Do not use! (Jaw) Version: (uncommissioned)
Energy: 6 MV
Geometry: SSD = 100 cm Field: 2 X 2

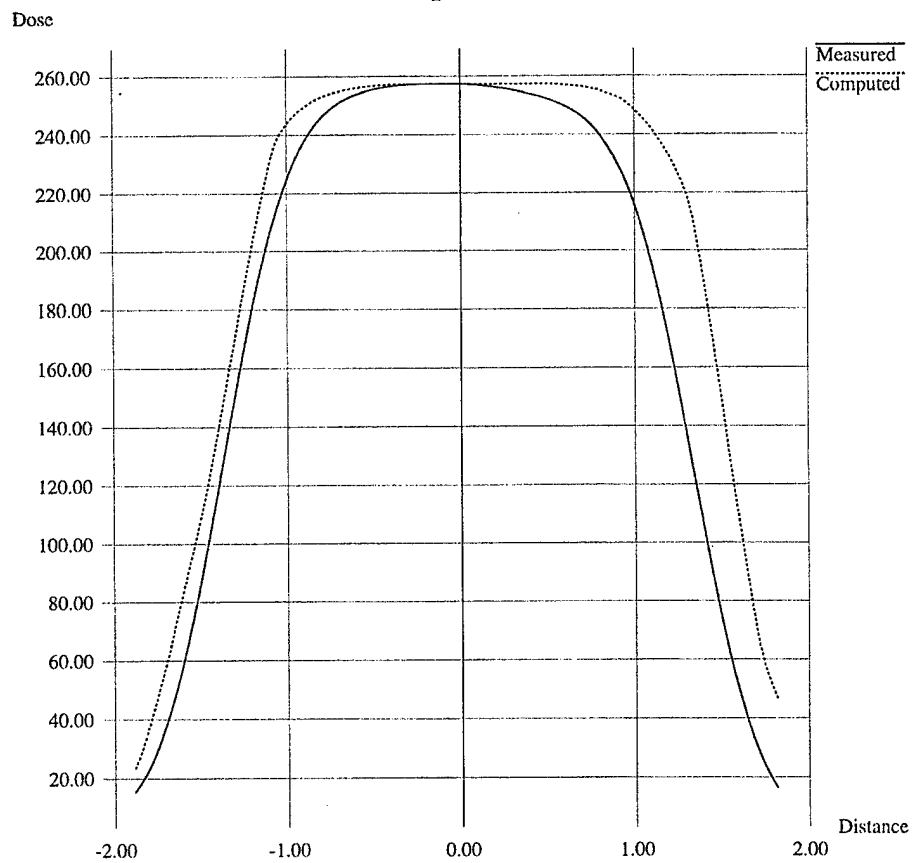
X: Depth= 1.50



Pinnacle³
Printed 07/07/04

Machine: Do not use! (Jaw) Version: (uncommissioned)
Energy: 6 MV
Geometry: SSD = 100 cm Field: 3 X 3

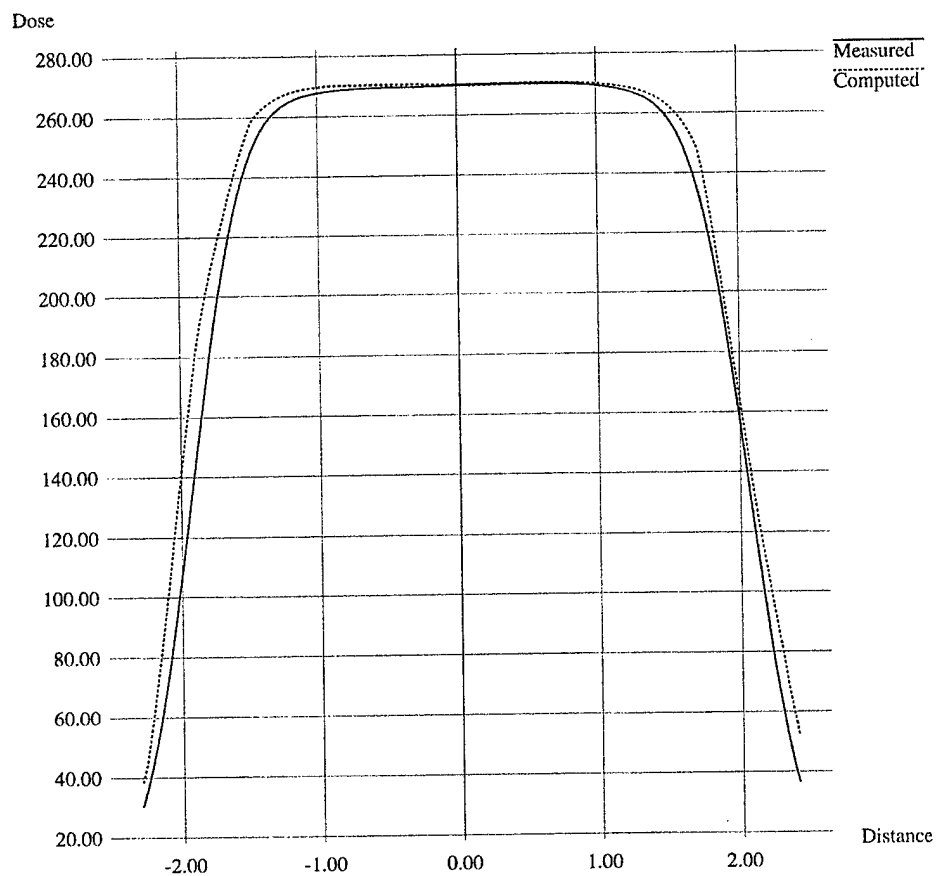
X: Depth= 1.50



Pinnacle³
Printed 07/07/04

Machine: Do not use! (Jaw) Version: (uncommissioned)
Energy: 6 MV
Geometry: SSD = 100 cm Field: 4 X 4

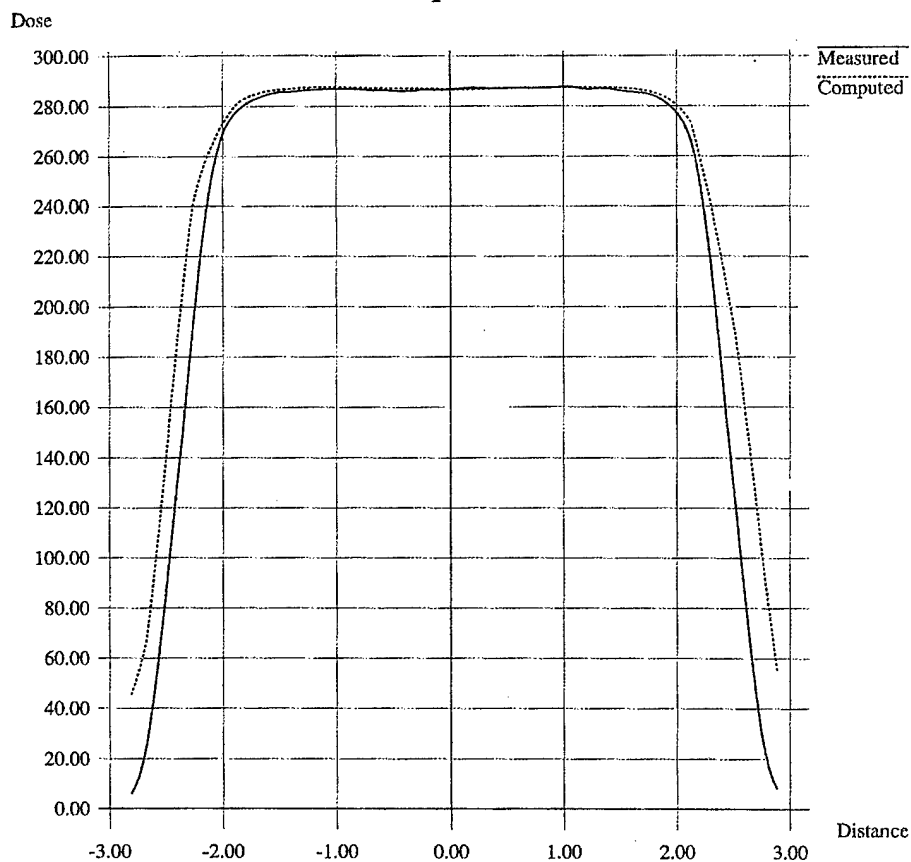
X: Depth= 1.50



Pinnacle³
Printed 07/07/04

Machine: Do not use! (Jaw) Version: (uncommissioned)
Energy: 6 MV
Geometry: SSD = 100 cm Field: 5 X 5

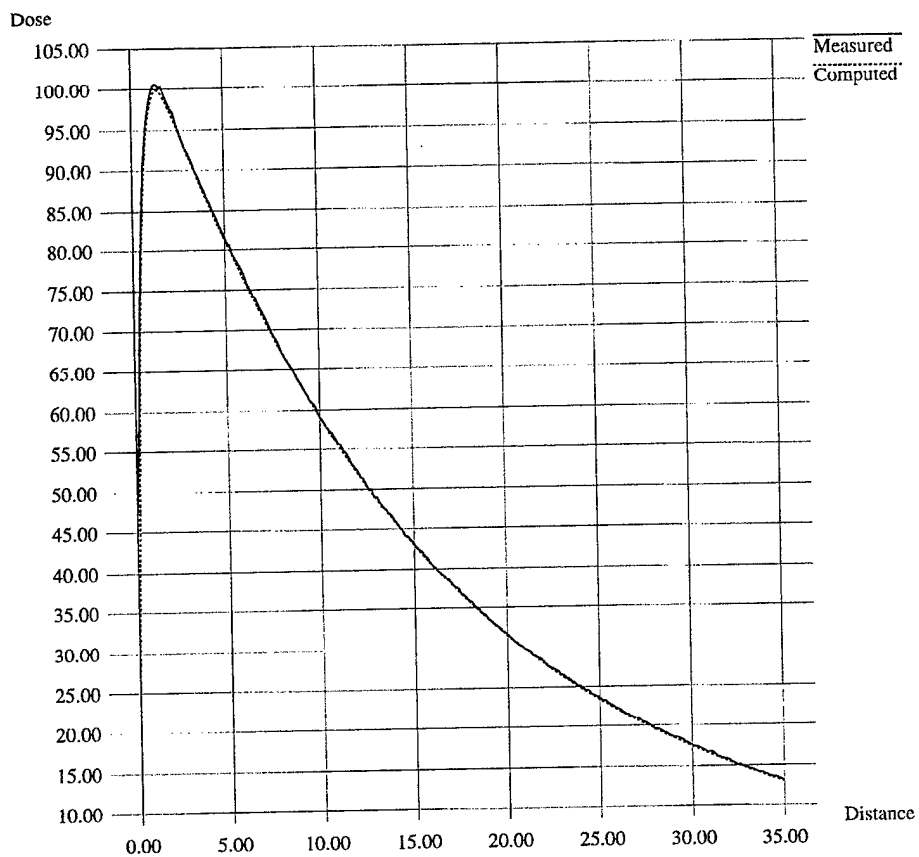
X: Depth= 1.50



Pinnacle³
Printed 07/31/04

Machine: DO NOT USE! JAW2 Version: (uncommissioned)
Energy: 6 MV
Geometry: SSD = 100 cm Field: 2 X 2

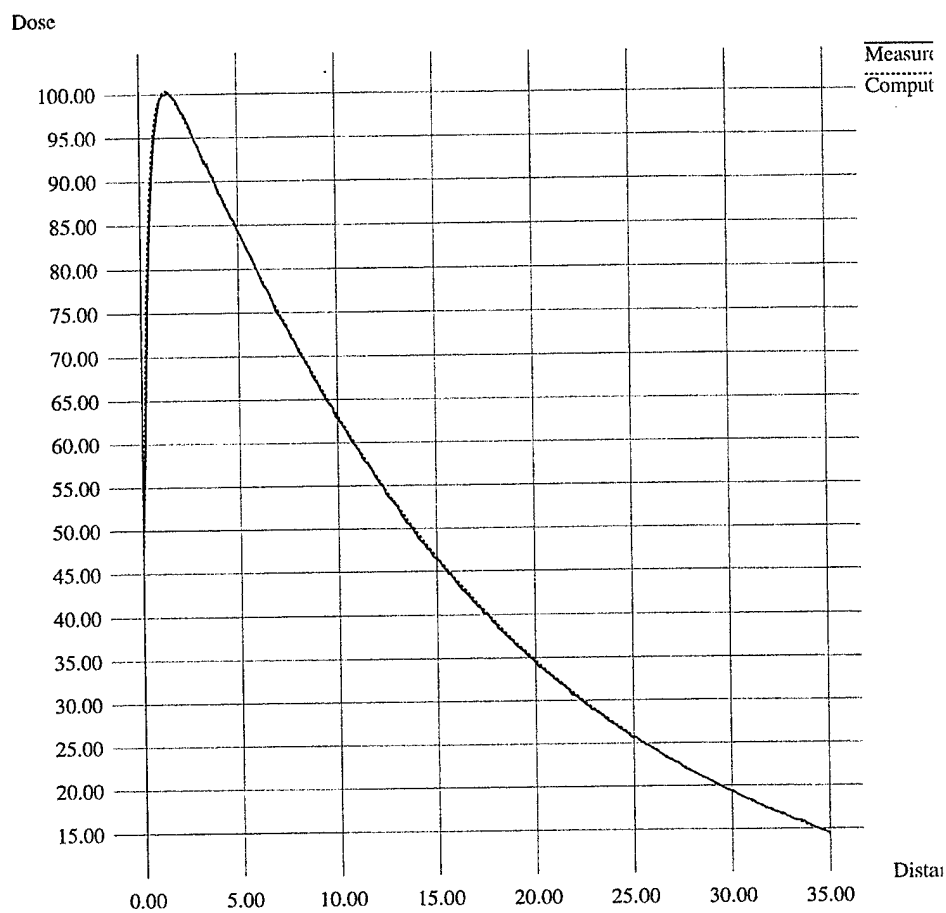
Depth Dose



Pinnacle³
Printed 07/31/04

Machine: DO NOT USE! JAW2 Version: (uncommissioned)
Energy: 6 MV
Geometry: SSD = 100 cm Field: 5 X 5

Depth Dose



B. MLC PROFILES

The following figures (8-12) are beam profiles generated by the measured data using the MLC for collimation, and compared to the ADAC model. Figures 13 and 14 represent depth dose data comparisons for the 2 cm² and 5 cm² field sizes.

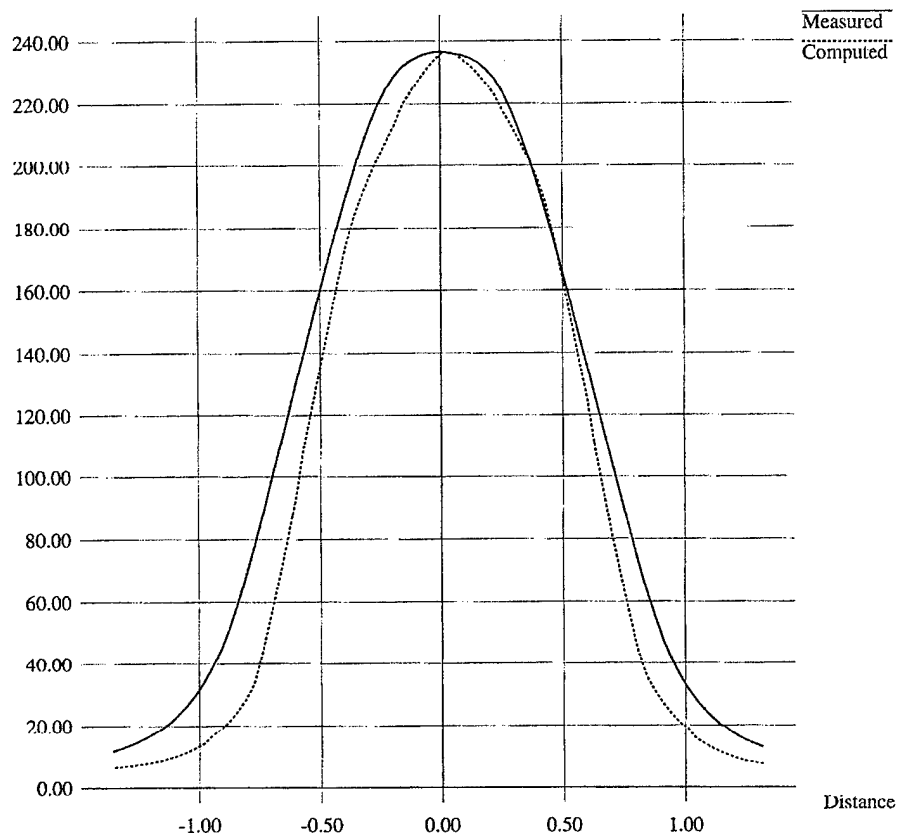
For the 1 cm² field size the measured data from MLC collimation varied from ADAC by a range of 2% - 12% along the central 50% of the beam. The MLC dose profile was consistently greater above the 50% maximum dose point. Below that dose point ADAC predicted a narrower penumbra than actually measured. For 2 cm² and 3 cm² field sizes there was good agreement between ADAC and MLC data with a difference of 2%-4% overall. For the 4 cm² and 5 cm² it was interesting to see that the MLC data reflected a profile consistently less than the ADAC model predicted. The depth dose comparison shows good agreement between the MLC and ADAC model.

Pinnacle³
Printed 07/21/04

Machine: Do not use! (MLC) Version: (uncommissioned)
Energy: 6 MV MLC
Geometry: SSD = 100 cm Field: 1 X 1

X: Depth= 1.50

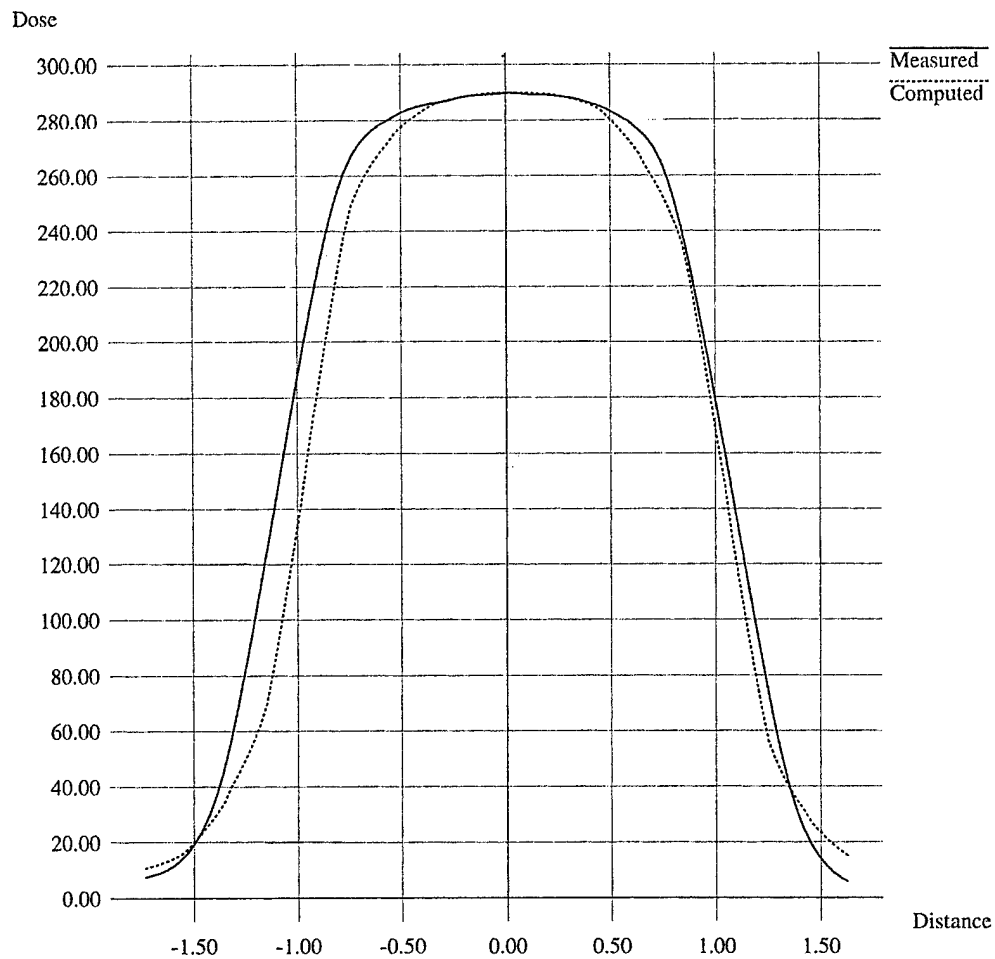
Dose



Pinnacle³
Printed 07/07/04

Machine: Do not use! (MLC) Version: (uncommissioned)
Energy: 6 MV MLC
Geometry: SSD = 100 cm Field: 2 X 2

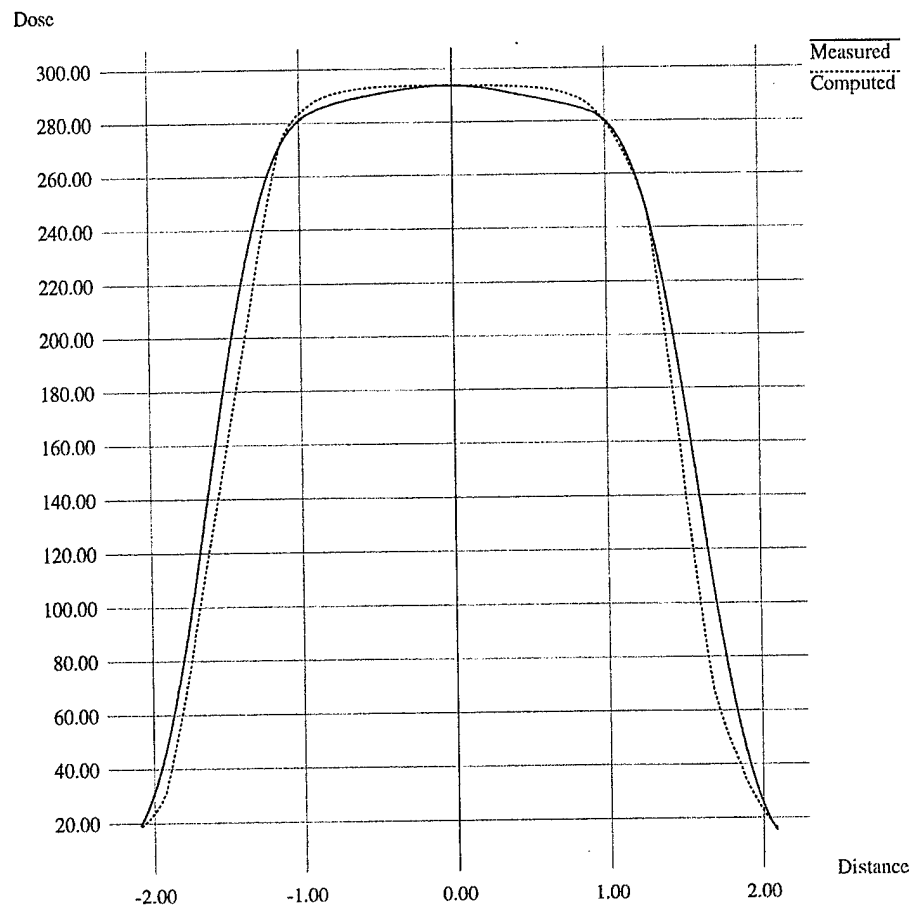
X: Depth= 1.50



Pinnacle³
Printed 07/07/04

Machine: Do not use! (MLC) Version: (uncommissioned)
Energy: 6 MV MLC
Geometry: SSD = 100 cm Field: 3 X 3

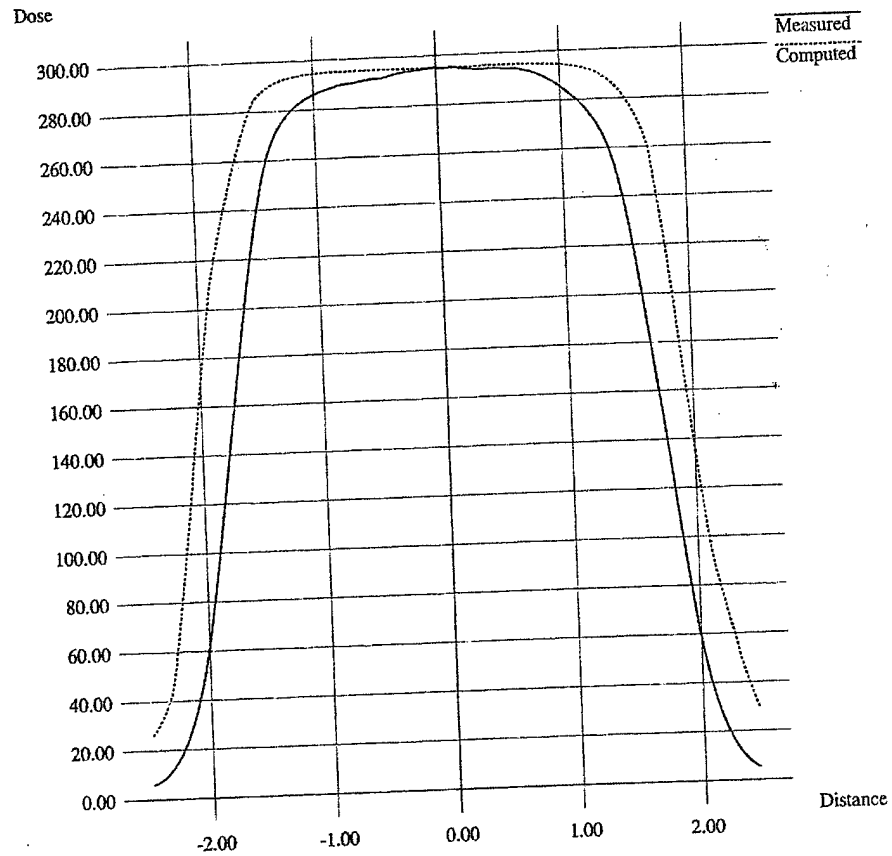
X: Depth= 1.50



Pinnacle³
Printed 07/07/04

Machine: Do not use! (MLC) Version: (uncommissioned)
Energy: 6 MV MLC
Geometry: SSD = 100 cm Field: 4 X 4

X: Depth= 1.50

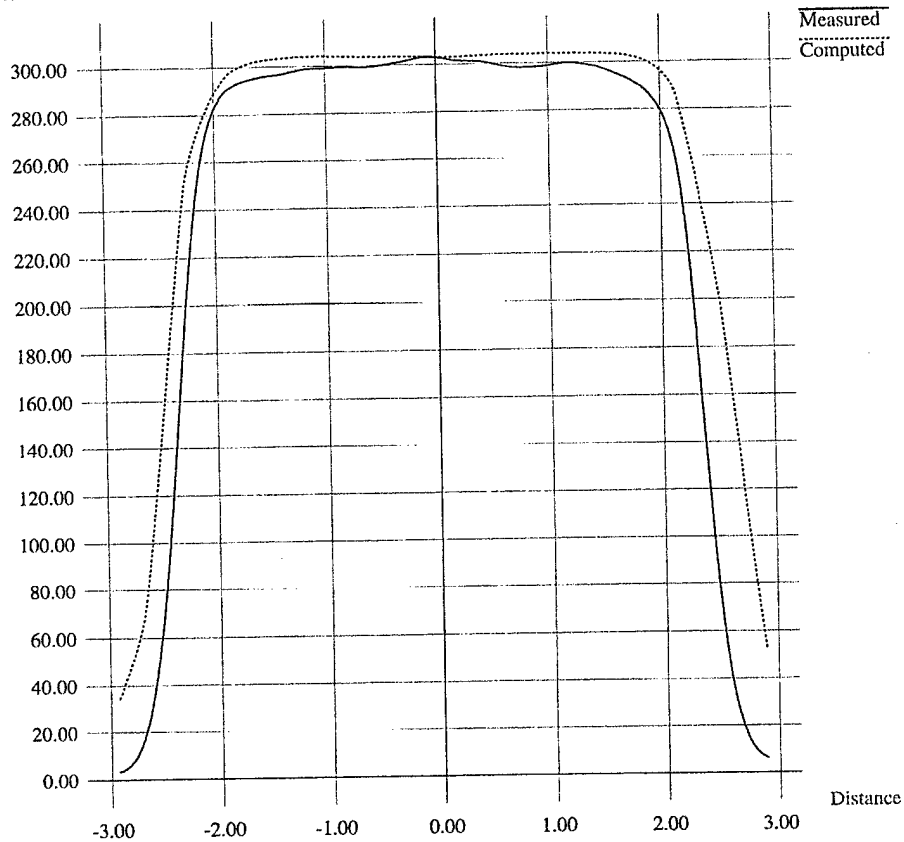


Pinnacle³
Printed 07/07/04

Machine: Do not use! (MLC) Version: (uncommissioned)
Energy: 6 MV MLC
Geometry: SSD = 100 cm Field: 5 X 5

X: Depth= 1.50

Dose

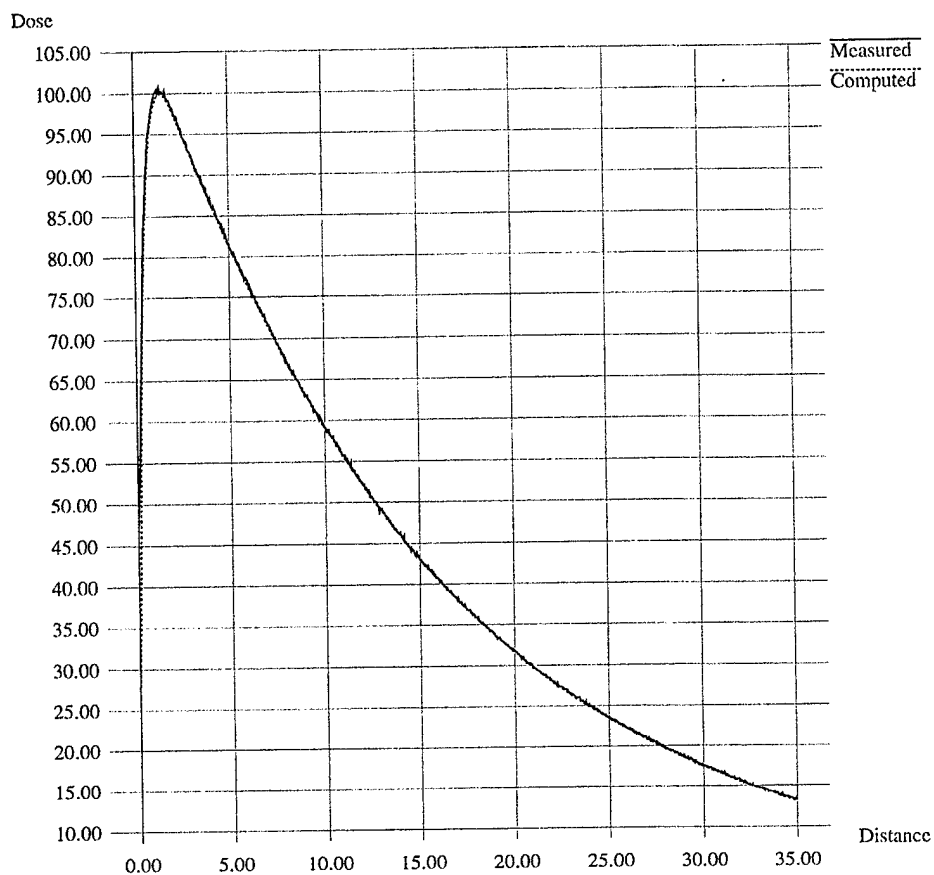


Distance

Pinnacle³
Printed 07/31/04

Machine: DO NOT USE! MLC2 Version: (uncommissioned)
Energy: 6 MV
Geometry: SSD = 100 cm Field: 2 X 2

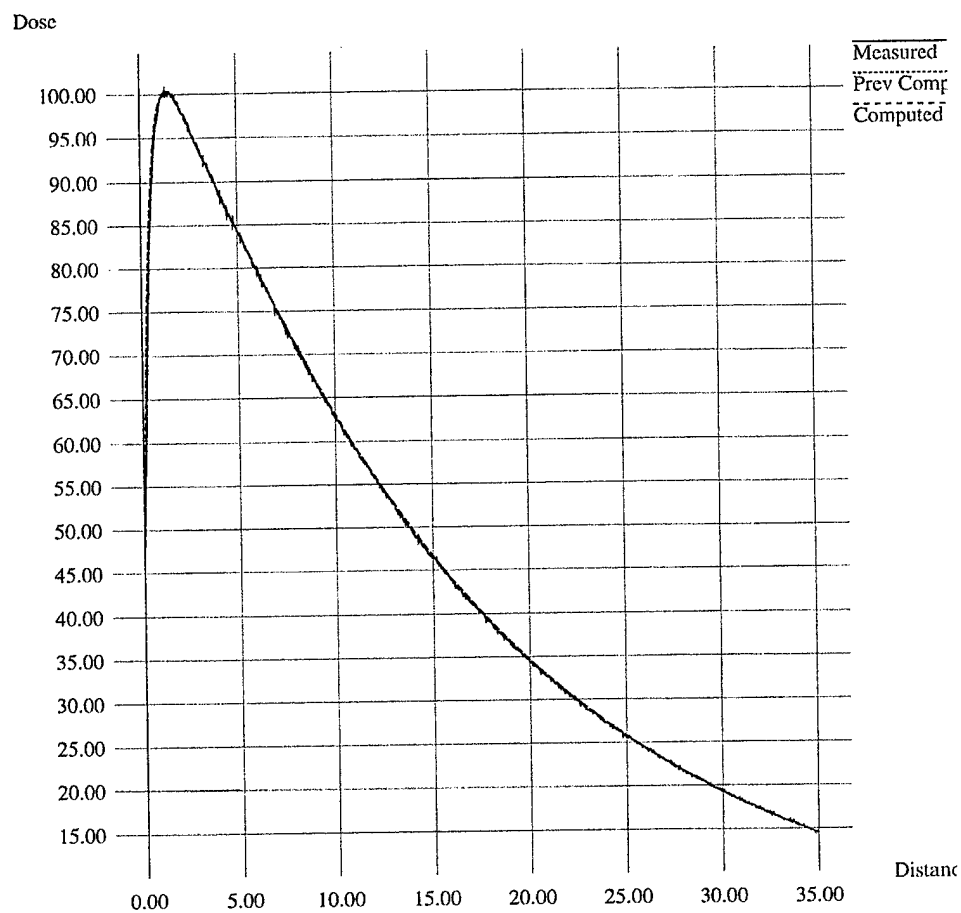
Depth Dose



Pinnacle³
Printed 07/31/04

Machine: DO NOT USE! MLC2 Version: (uncommissioned)
Energy: 6 MV
Geometry: SSD = 100 cm Field: 5 X 5

Depth Dose



C. HEAD AND NECK PLANAR DOSE DATA AND IMAGES

1. COMPARISON OF PLANAR IMAGES

The following figures (15-17) are planar images of a right lateral neck view from an actual head and neck IMRT plan. The first image represents the ADAC model. The following images reflect the same view but using the Jaw model and MLC model respectively.

Planar Dose Computation

Planar Dose Options

Trial: Opt-IMRT

Dose Planes: DosePlane_1

Name: DosePlane_1

Beam: RT-LAT-NECI

Beam SSD: 95.66 cm

☒ Flat water phantom ☐ Patient data

SPD: 100 cm

SSD: 96.5 cm

	X	Y
Pixel Size	0.100 cm	0.100 cm
Dimension	100 px	100 px
Color	greyscale	
Dose Units	cGy/MU	

Status:

Export Planar Dose

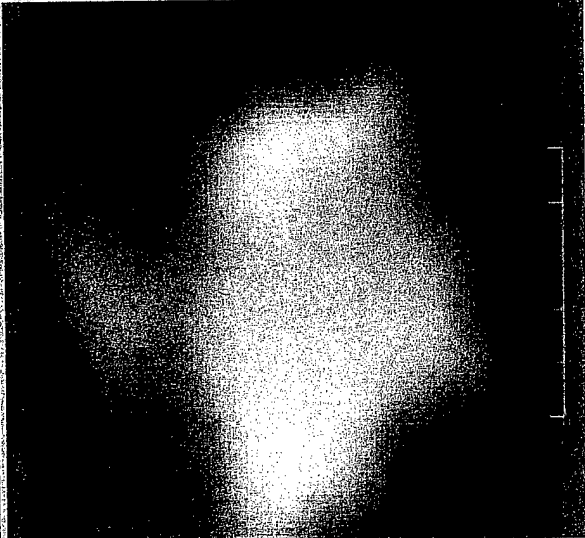
Directory: floppy/floppy0

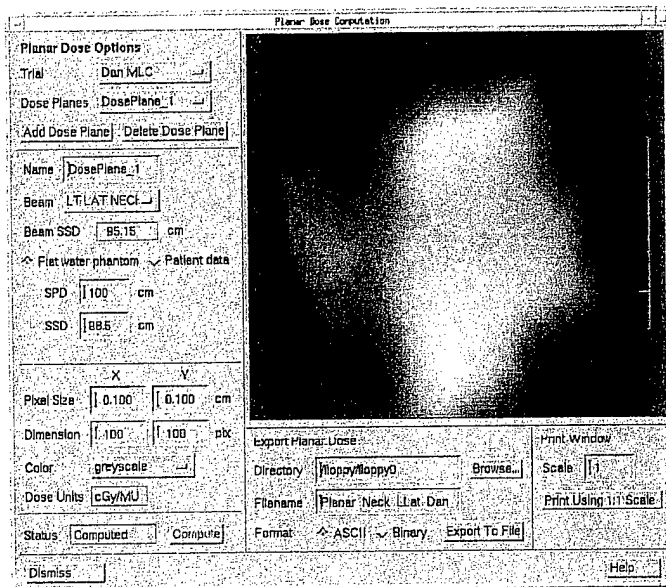
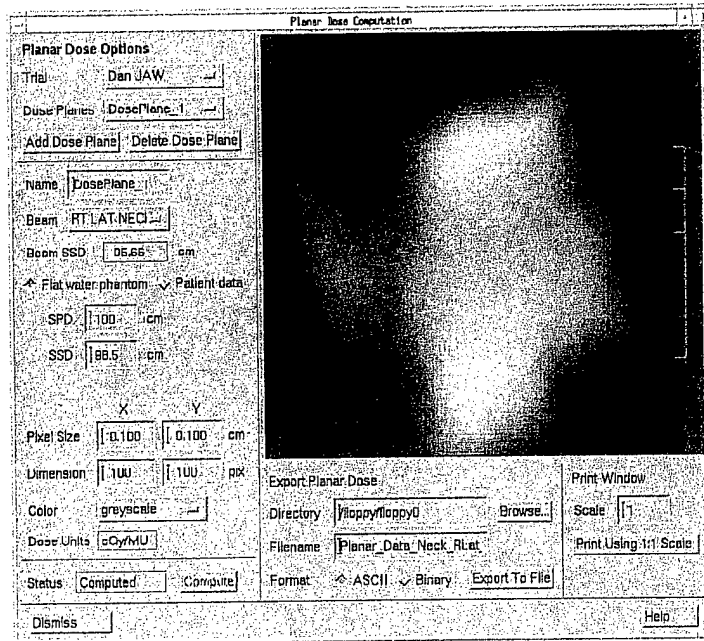
Filename: Planar_Neck_LLat_Opt_1

Format: ☒ ASCII ☐ Binary

Print Window

Scale: 1

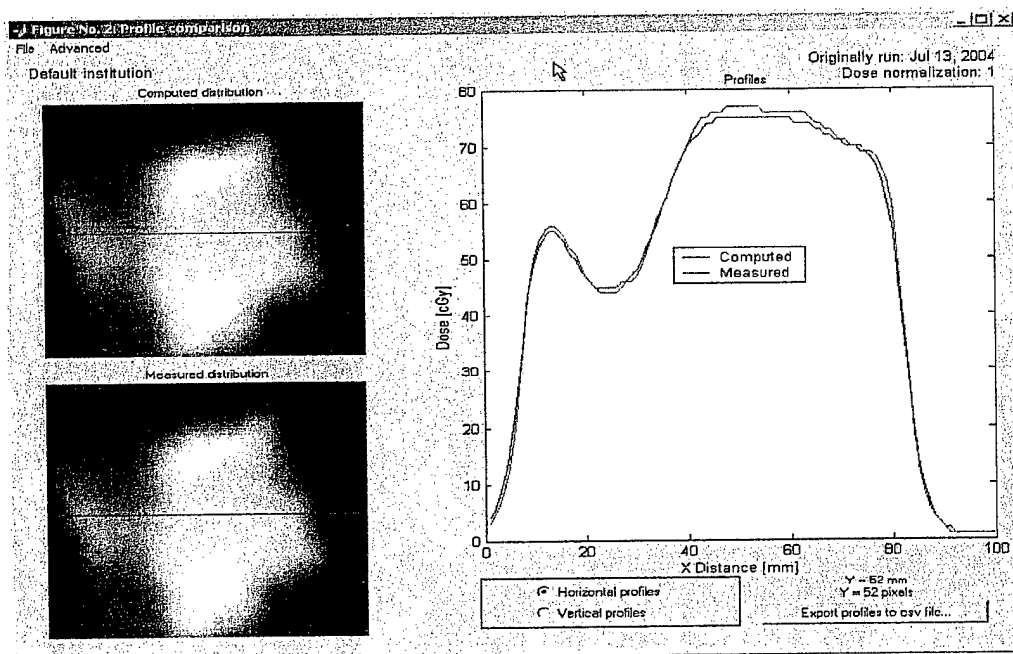
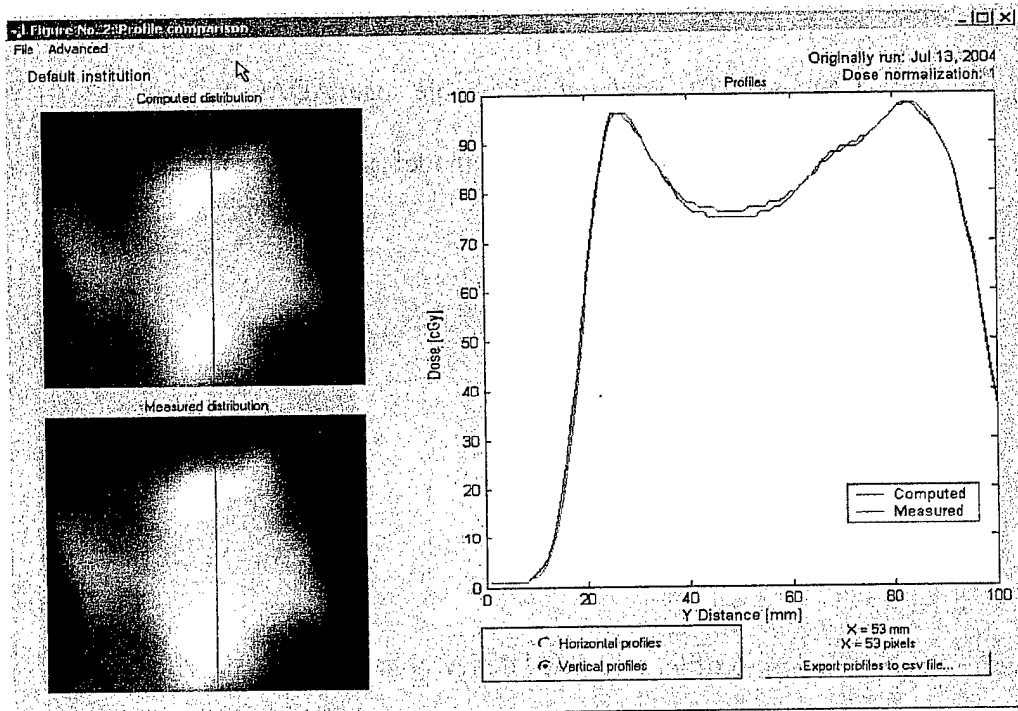


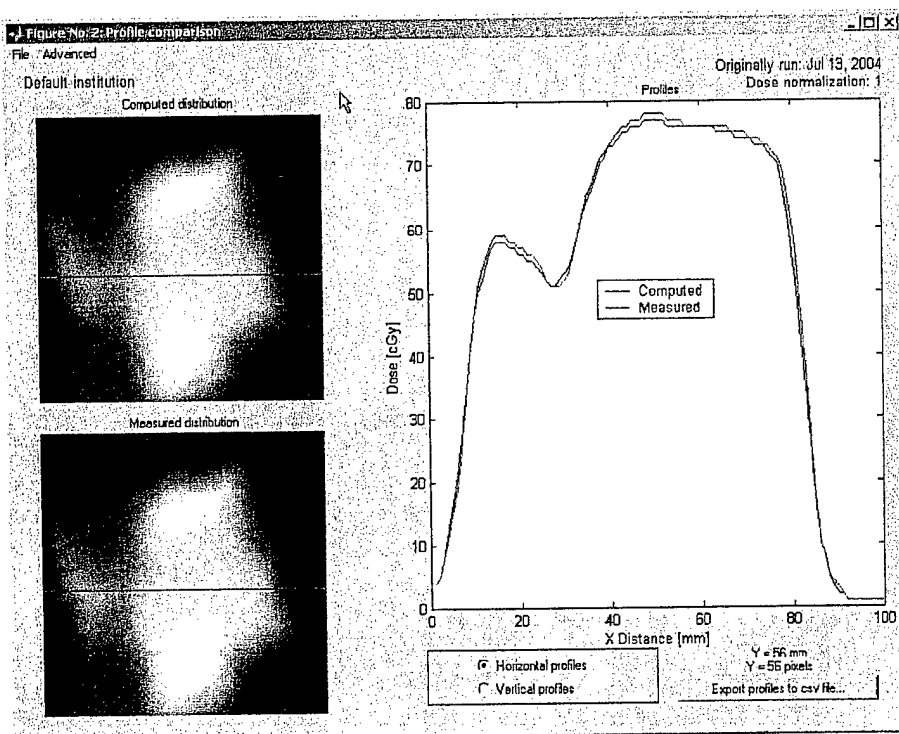
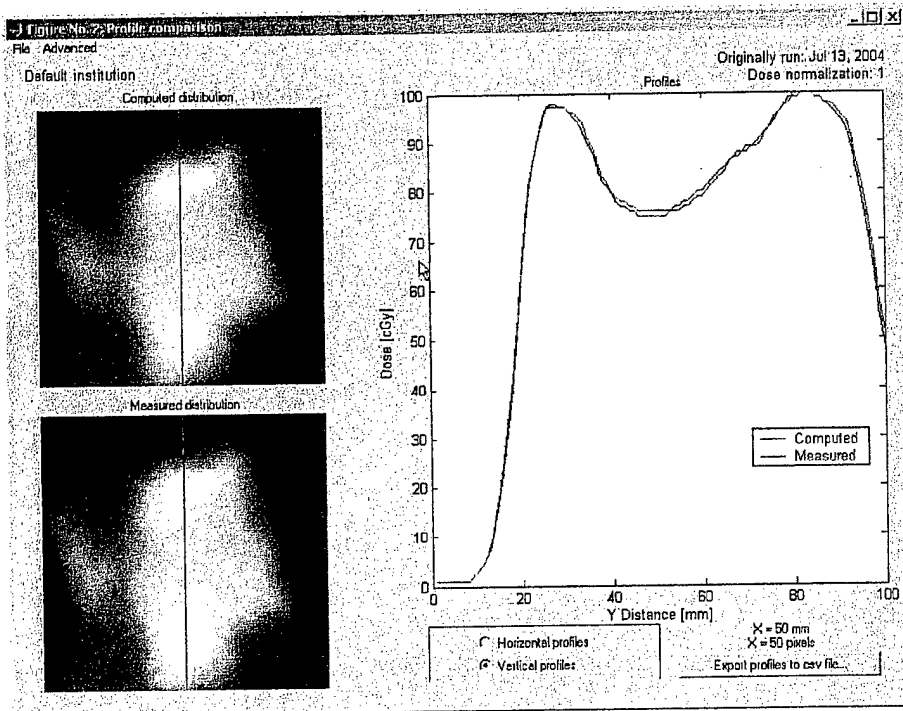


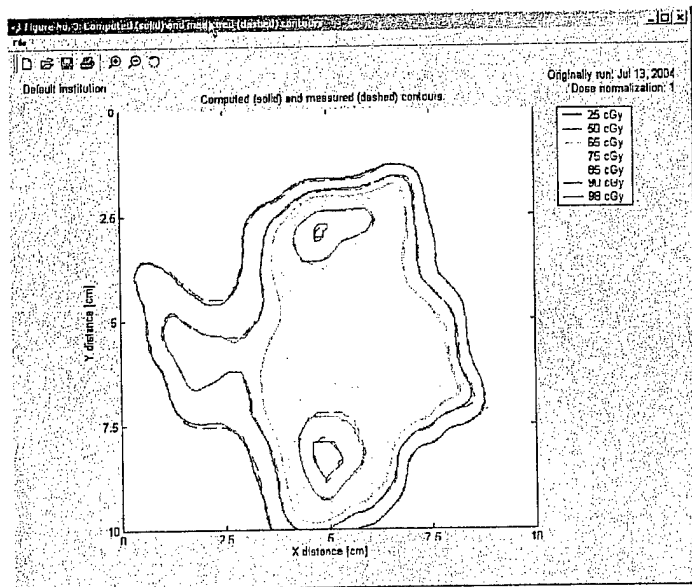
The images visually reflect slight variations but there is overall good agreement between all three models used.

2. COMPARISON OF CALCULATED DELIVERABLE DATA

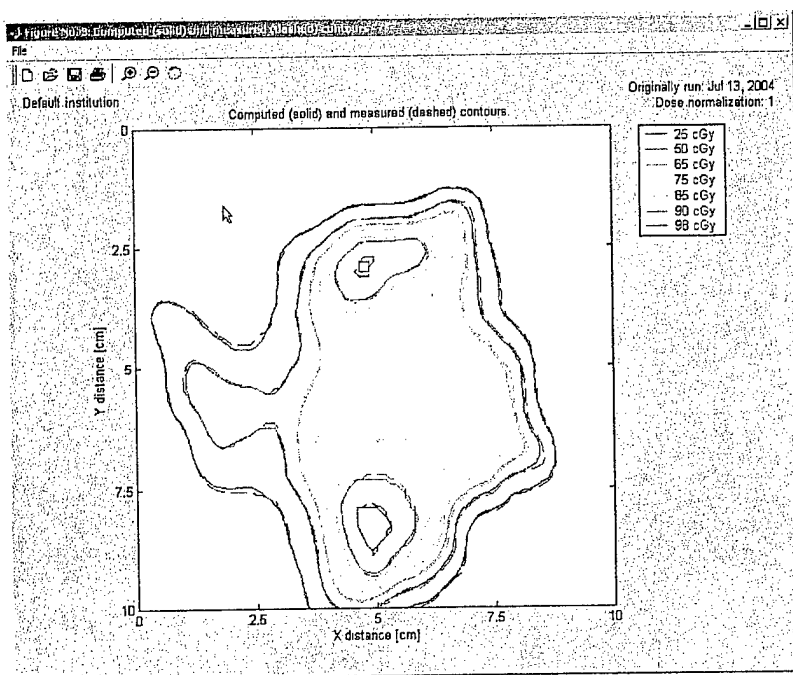
Figure 18 represents a vertical dose profile comparison of the calculated deliverable data using the ADAC model versus the Jaw model.







There is some variation between the two at the 75cGy and higher isodose lines.

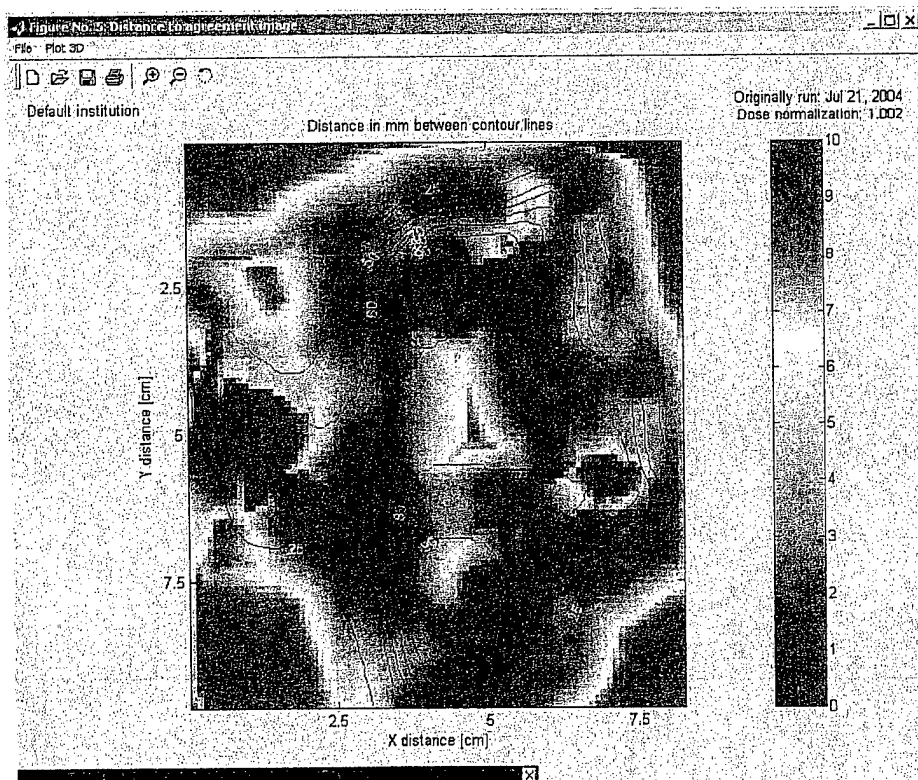


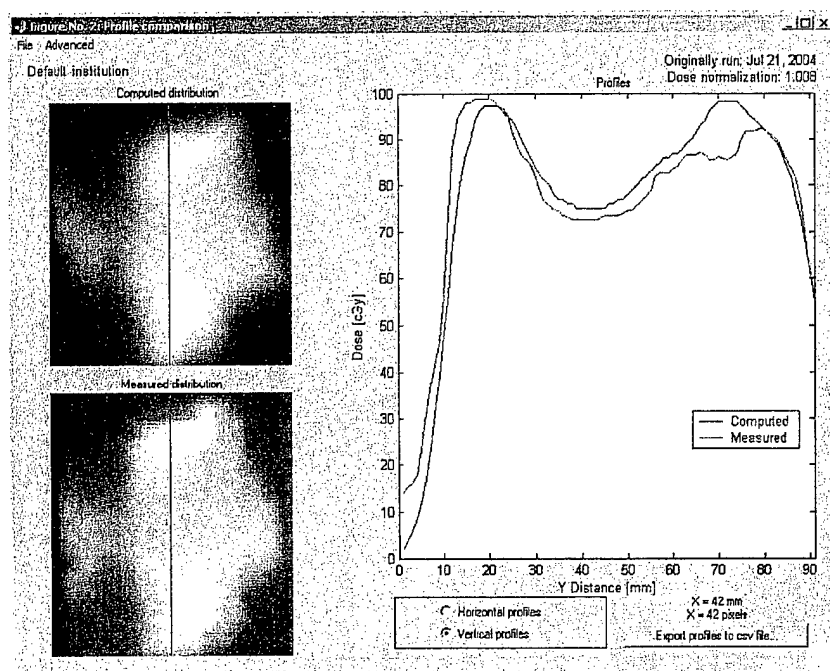
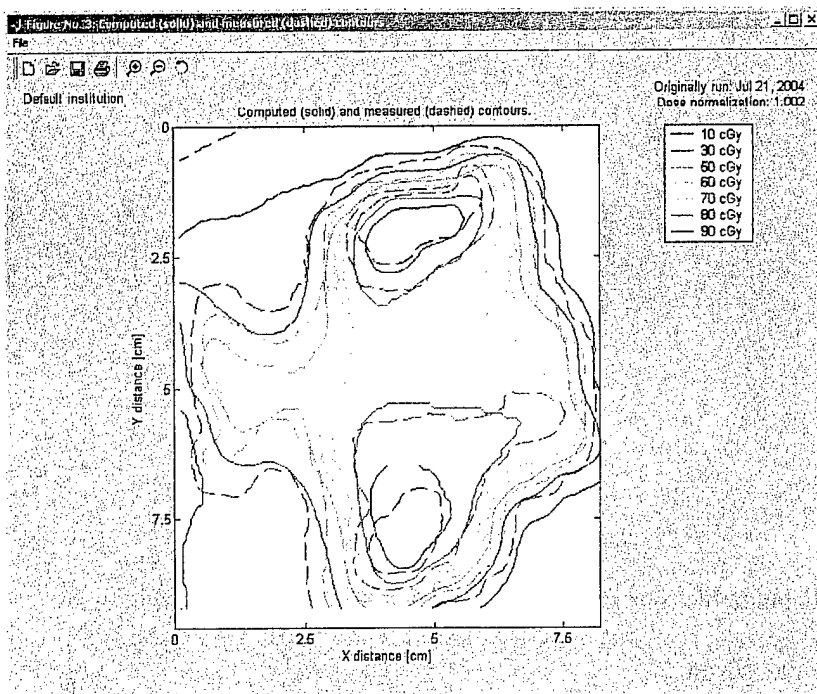
There is some difference at the 85cGy and higher isodose lines.

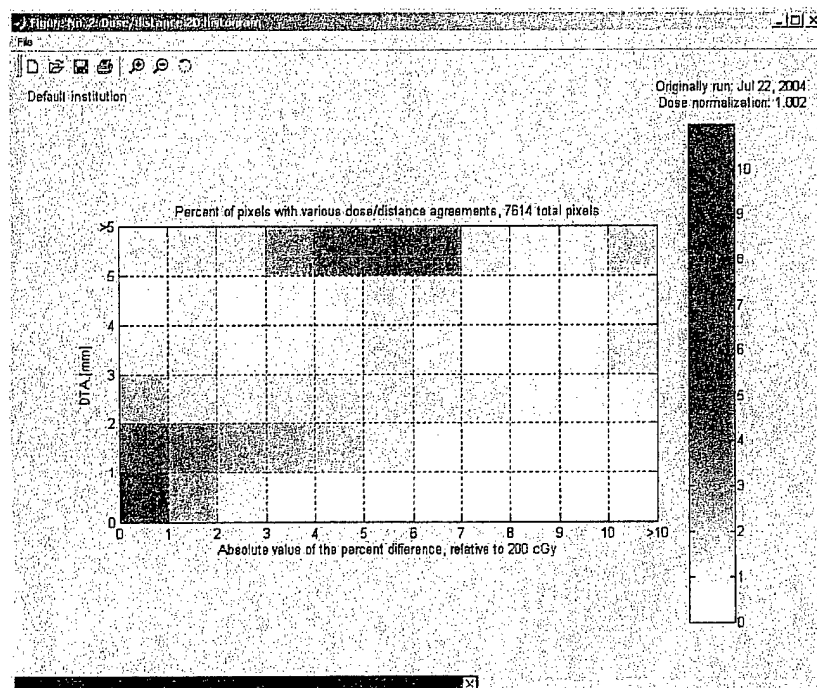
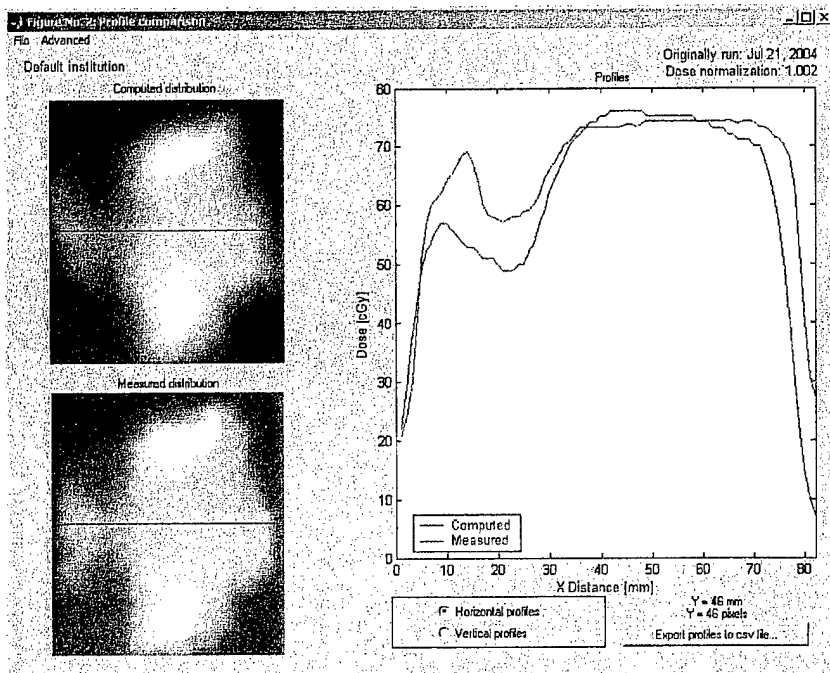
3. COMPARISON OF CALCULATED DELIVERABLE VS. DELIVERABLE MEASURED DATA

To determine which model best predicted its measured dose from film, the calculated deliverable data was compared to the deliverable measured data for each model. The following figures represent this series of comparisons. All compare the same right lateral neck IMRT view.

Figures 24-29 represent the tests used to compare the ADAC model calculated deliverable plan versus the ADAC model deliverable measured data from film.

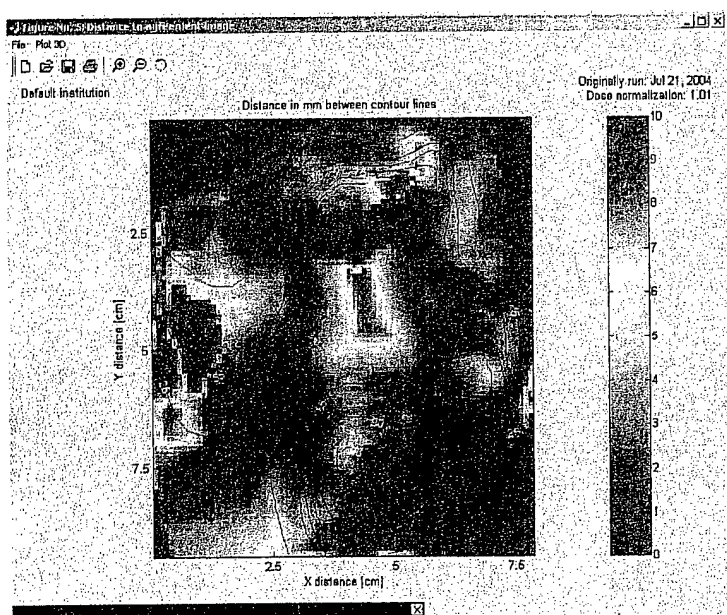
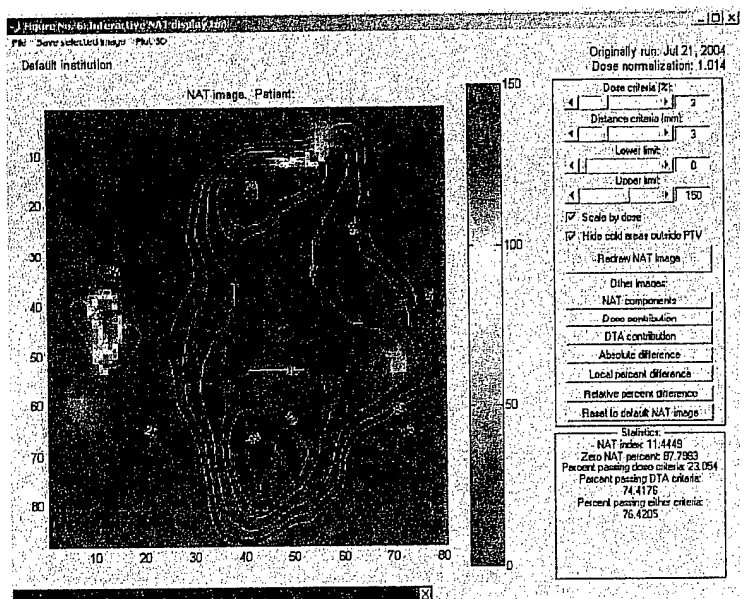


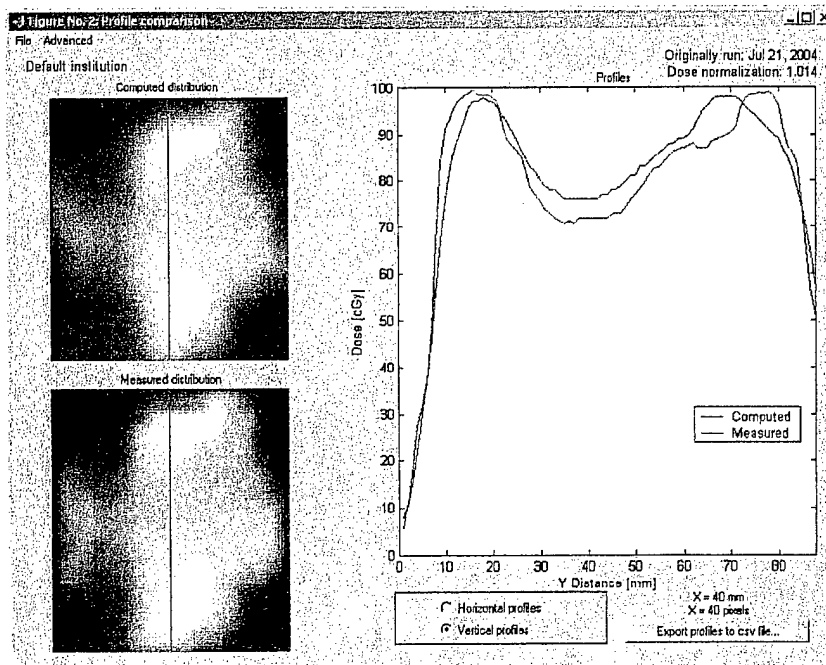
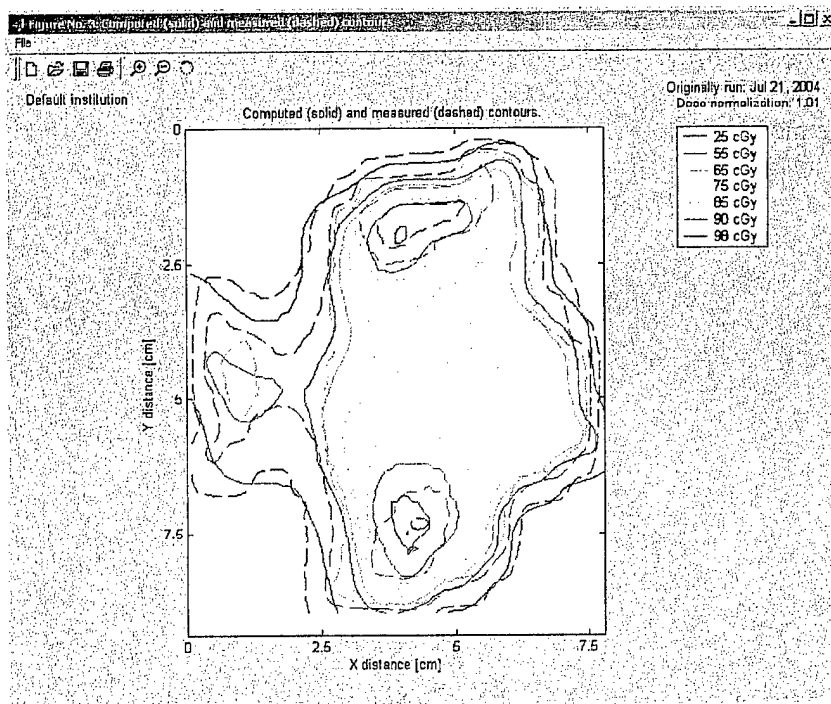


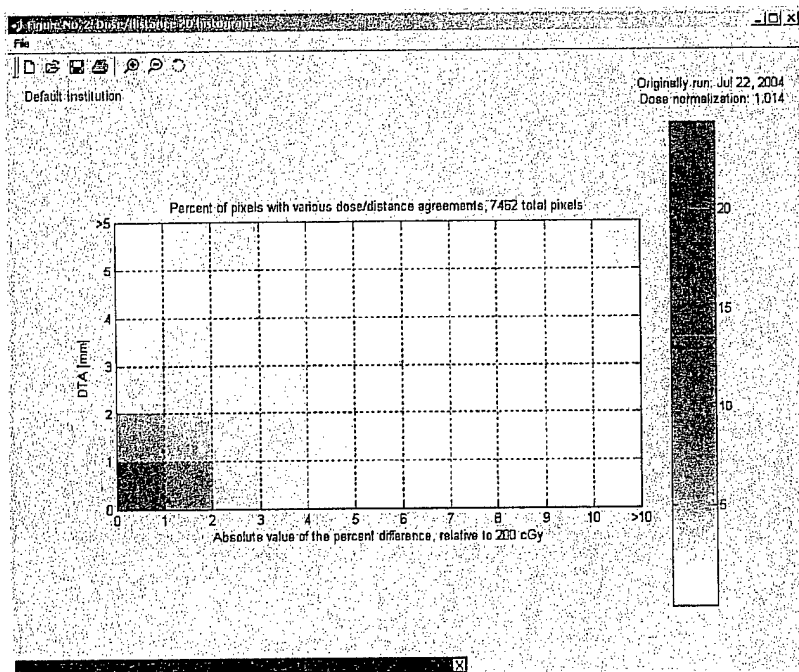
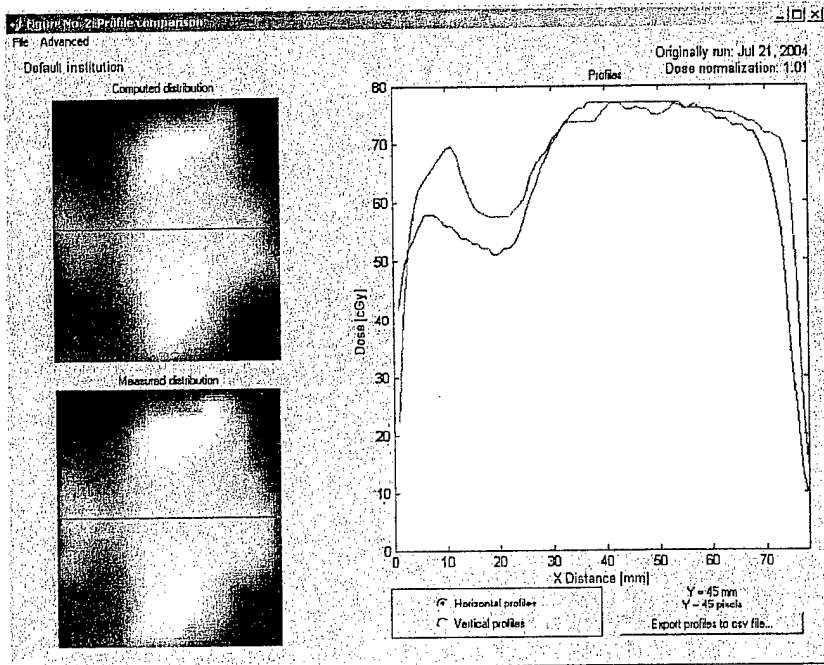


When comparing the ADAC calculated deliverable plan versus the ADAC deliverable measured data, the DTA scores were only in the 50% range. There is noticeable dose difference noted in the left side of the DTA and NAT images. When viewing the 2D dose histogram, there are a significant amount of pixels which fall outside the thresholds of 3% or 3mm.

Figures 30-35 represent the comparison between the MLC calculated deliverable plan versus the MLC deliverable measured data from film.

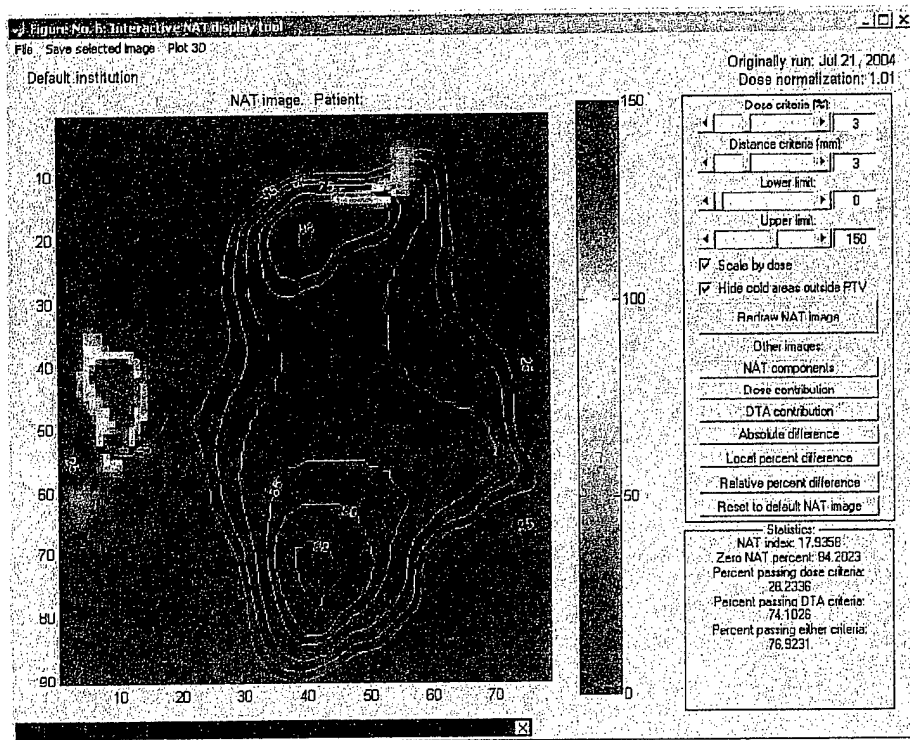


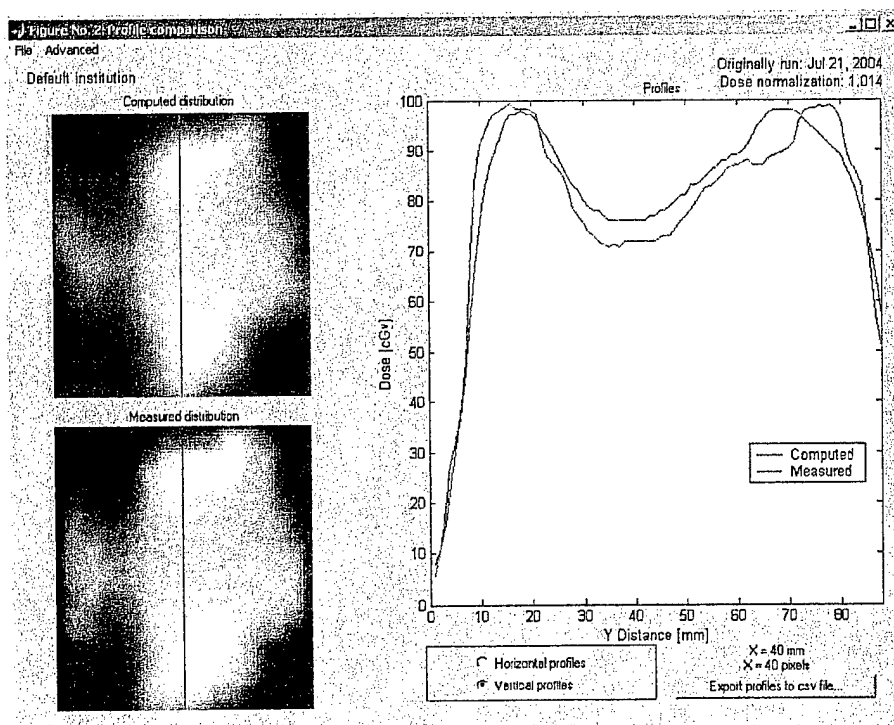
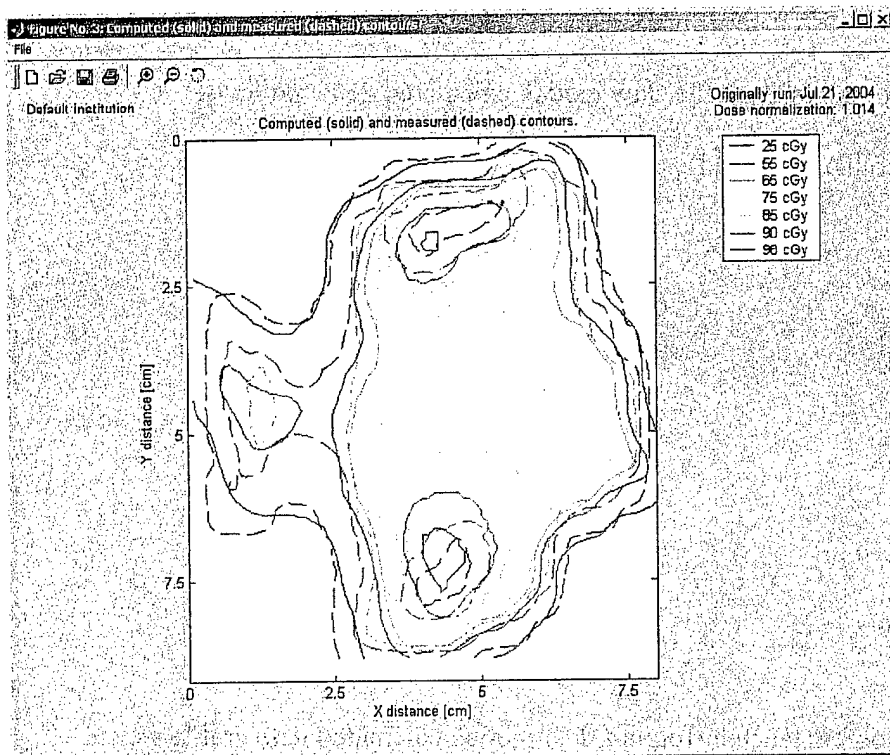


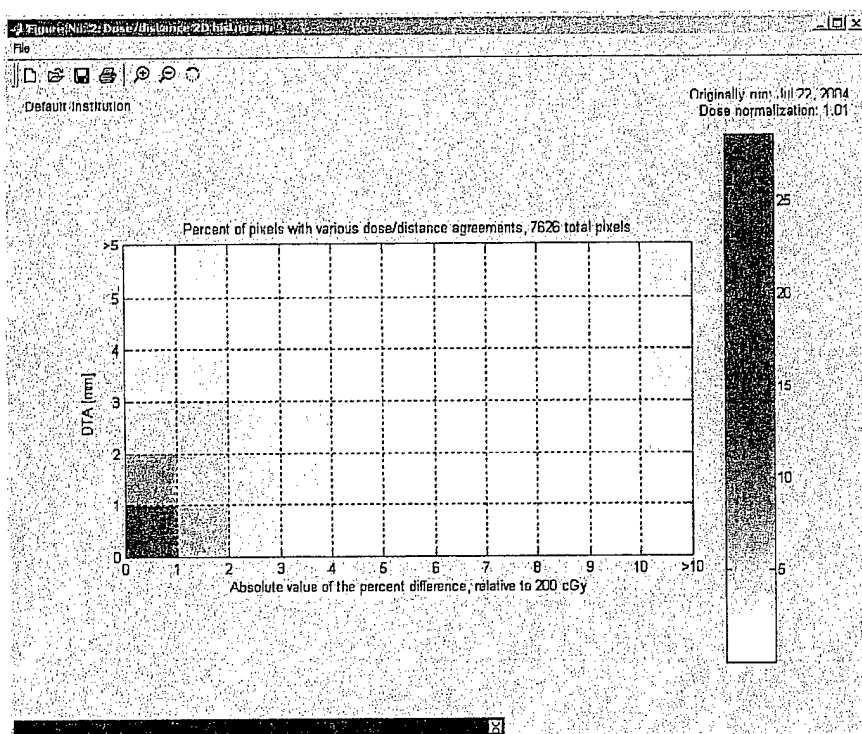
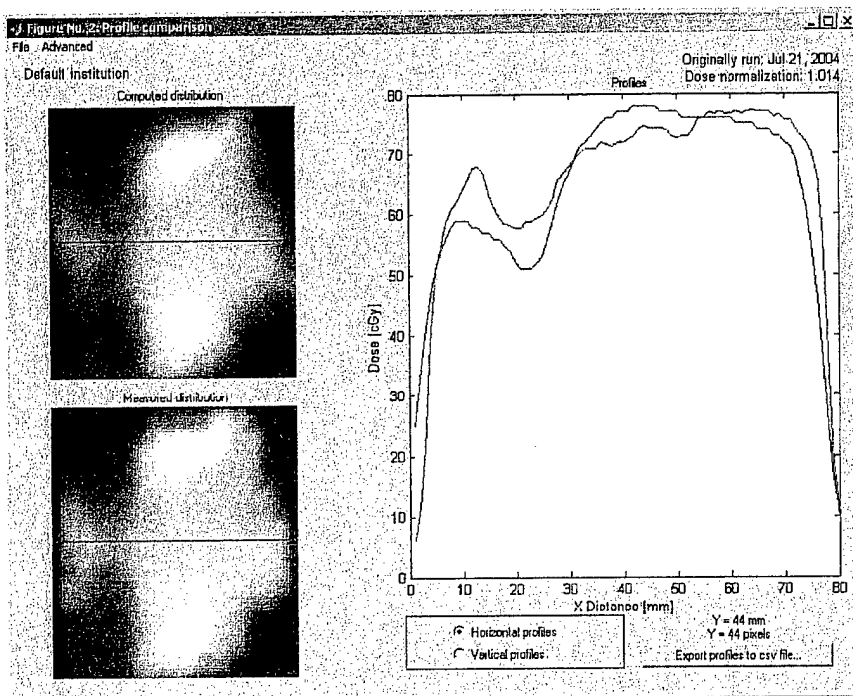


With the distance to agreement scores in the 70% range, the MLC model was a better predictor for its measured data than the ADAC model was for its measured data.

Figures 36-41 represent the comparison between the Jaw model calculated deliverable dose versus the deliverable measured data.







The distance to agreement scores were as high as the MLC comparison. The Jaw model was a better predictor for its measured data than the ADAC model was for its measured data. The following summarizes the NAT and DTA scores for the models.

Calculated deliverable vs. deliverable measured from film

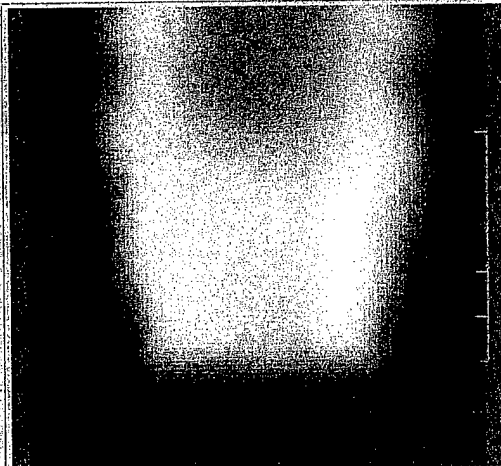
	NAT Index	Zero NAT %	% passing NAT criteria	% passing DTA criteria	% passing either criteria
ADAC Model	36.49	58.89	21.14	50.32	53.72
MLC Model	11.44	87.8	23.05	74.42	76.42
Jaw Model	17.94	84.2	28.23	74.1	76.92

D. PROSTATE PLANAR DOSE DATA AND IMAGES

1. COMPARISON OF PLANAR IMAGES

The following figures (43-45) are planar images of a posterior to anterior view from an actual prostate IMRT plan. The first image represents the ADAC model. The following images reflect the same view but using the Jaw model and MLC model respectively.

Planar Dose Computation																					
Planar Dose Options: Trial: <input type="text" value="IMRT's Ild"/> Dose Planes: <input type="text" value="DosePlane1"/> <input type="button" value="Add Dose Plane"/> <input type="button" value="Delete Dose Plane"/>																					
Name: <input type="text" value="DosePlane1"/> Beam: <input type="text" value="PA 180"/> Beam SSD: <input type="text" value="89.26"/> cm Flat water phantom <input checked="" type="checkbox"/> Patient data <input type="checkbox"/> SPD: <input type="text" value="100"/> cm SSD: <input type="text" value="88.5"/> cm																					
<table border="1"> <thead> <tr> <th></th> <th>X</th> <th>Y</th> <th></th> </tr> </thead> <tbody> <tr> <td>Pixel Size</td> <td><input type="text" value="0.100"/></td> <td><input type="text" value="0.100"/></td> <td>cm</td> </tr> <tr> <td>Dimension</td> <td><input type="text" value="100"/></td> <td><input type="text" value="100"/></td> <td>px</td> </tr> <tr> <td>Color</td> <td colspan="3"><input type="text" value="grayscale"/></td> </tr> <tr> <td>Dose Units</td> <td colspan="3"><input type="text" value="cGy/MU"/></td> </tr> </tbody> </table>			X	Y		Pixel Size	<input type="text" value="0.100"/>	<input type="text" value="0.100"/>	cm	Dimension	<input type="text" value="100"/>	<input type="text" value="100"/>	px	Color	<input type="text" value="grayscale"/>			Dose Units	<input type="text" value="cGy/MU"/>		
	X	Y																			
Pixel Size	<input type="text" value="0.100"/>	<input type="text" value="0.100"/>	cm																		
Dimension	<input type="text" value="100"/>	<input type="text" value="100"/>	px																		
Color	<input type="text" value="grayscale"/>																				
Dose Units	<input type="text" value="cGy/MU"/>																				
<table border="1"> <tr> <td>Status: <input type="text" value="Computed"/> <input type="button" value="Compute"/></td> <td> Export Planar Dose Directory: <input type="text" value="/floppy/floppy0"/> <input type="button" value="Browse..."/> Filename: <input type="text" value="Prostate_PA_IMRT5.txt"/> Format: <input checked="" type="radio"/> ASCII <input type="radio"/> Binary <input type="button" value="Export To File"/> </td> <td> Print Window Scale: <input type="text" value="1"/> <input type="button" value="Print Using 1:1 Scale"/> </td> </tr> </table>		Status: <input type="text" value="Computed"/> <input type="button" value="Compute"/>	Export Planar Dose Directory: <input type="text" value="/floppy/floppy0"/> <input type="button" value="Browse..."/> Filename: <input type="text" value="Prostate_PA_IMRT5.txt"/> Format: <input checked="" type="radio"/> ASCII <input type="radio"/> Binary <input type="button" value="Export To File"/>	Print Window Scale: <input type="text" value="1"/> <input type="button" value="Print Using 1:1 Scale"/>																	
Status: <input type="text" value="Computed"/> <input type="button" value="Compute"/>	Export Planar Dose Directory: <input type="text" value="/floppy/floppy0"/> <input type="button" value="Browse..."/> Filename: <input type="text" value="Prostate_PA_IMRT5.txt"/> Format: <input checked="" type="radio"/> ASCII <input type="radio"/> Binary <input type="button" value="Export To File"/>	Print Window Scale: <input type="text" value="1"/> <input type="button" value="Print Using 1:1 Scale"/>																			
<input type="button" value="Dismiss"/> <input type="button" value="Help"/>																					



Planar Dose Computation

Planar Dose Options

Trial: JAW.Dan

Dose Planes: DosePlane_1

Add Dose Plane Delete Dose Plane

Name: DosePlane_1

Beam: PA 180

Beam SSD: 88.26 cm

Flat water phantom Patient data

SPD: 100 cm

SSD: 88.5 cm

Pixel Size: X: 0.100 Y: 0.100 cm

Dimension: 150 150 pix

Color: greyscale

Dose Units: cGy/MU

Status: Computed Compute

Export Planar Dose

Directory: /tmp/py0 Browse

Filename: Planar_Data_Prost_PA_1

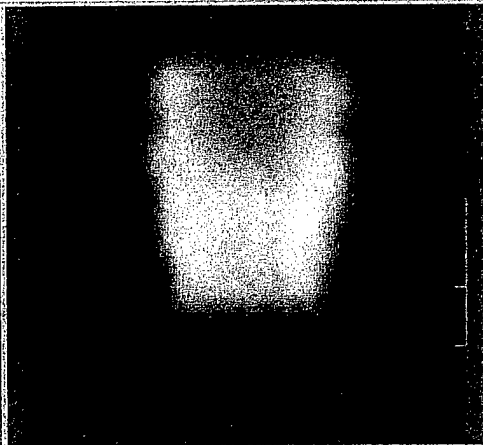
Format: ASCII Binary Export To File

Print Window

Scale: 1

Print Using 1:1 Scale

Dismiss Help



Planar Dose Computation

Planar Dose Options

Trial: MLC.Dan

Dose Planes: DosePlane_1

Add Dose Plane Delete Dose Plane

Name: DosePlane_1

Beam: PA 180

Beam SSD: 88.26 cm

Flat water phantom Patient data

SPD: 100 cm

SSD: 88.5 cm

Pixel Size: X: 0.100 Y: 0.100 cm

Dimension: 100 100 pix

Color: greyscale

Dose Units: cGy/MU

Status: Computed Compute

Export Planar Dose

Directory: /tmp/py0 Browse

Filename: Prostate_PA_MLC_DAN

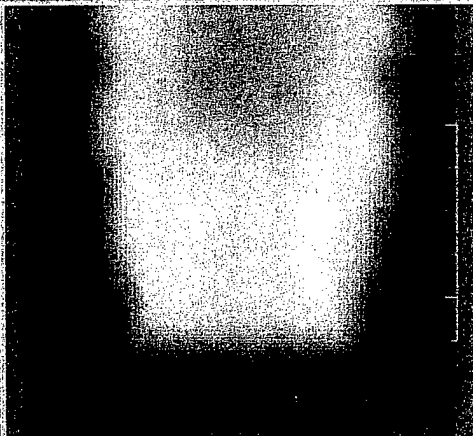
Format: ASCII Binary Export To File

Print Window

Scale: 1

Print Using 1:1 Scale

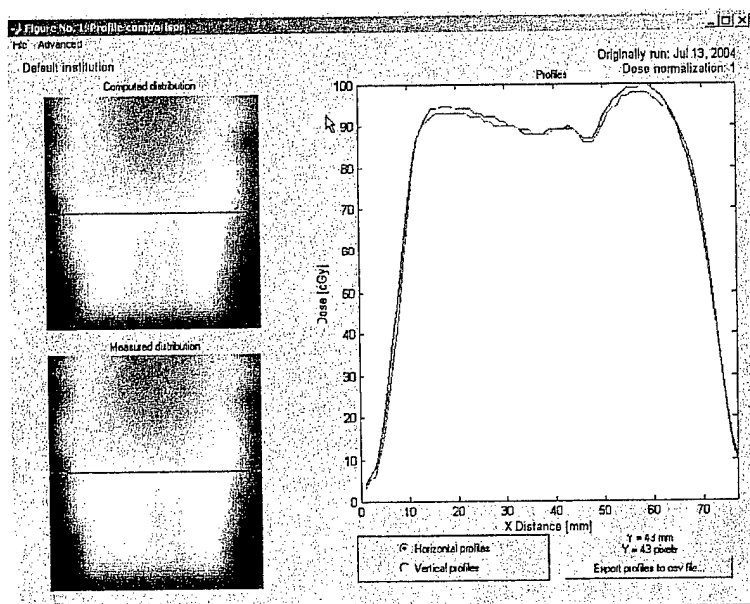
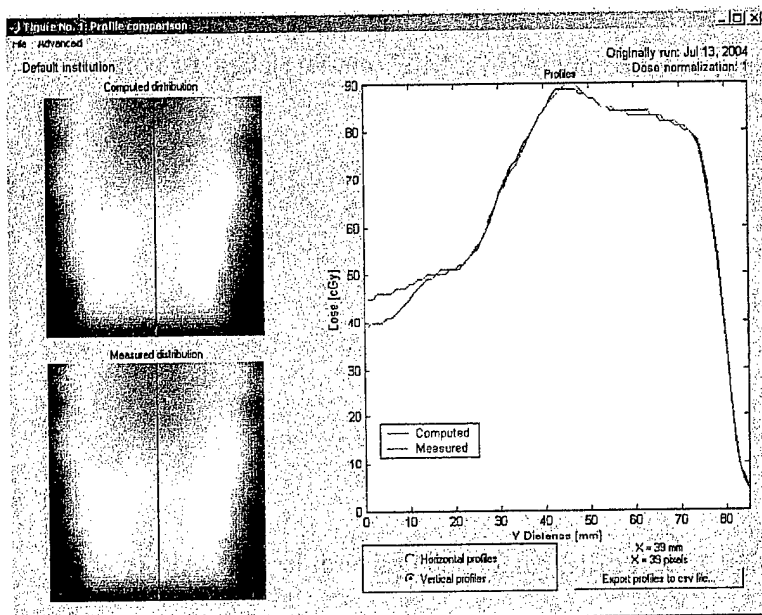
Dismiss Help

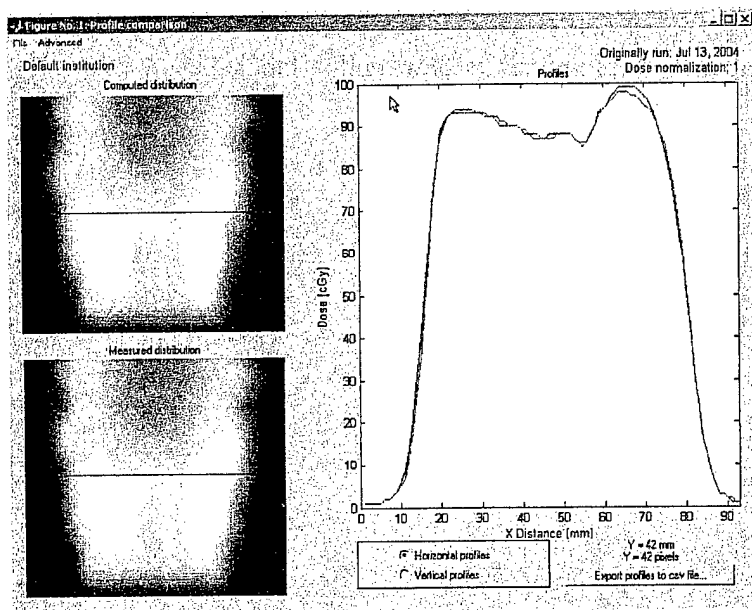
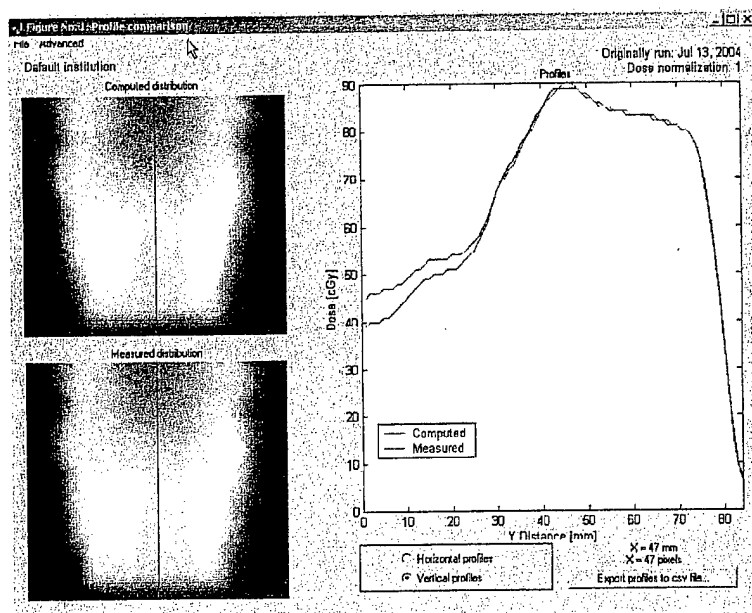


The images visually reflect good agreement between all three models used.

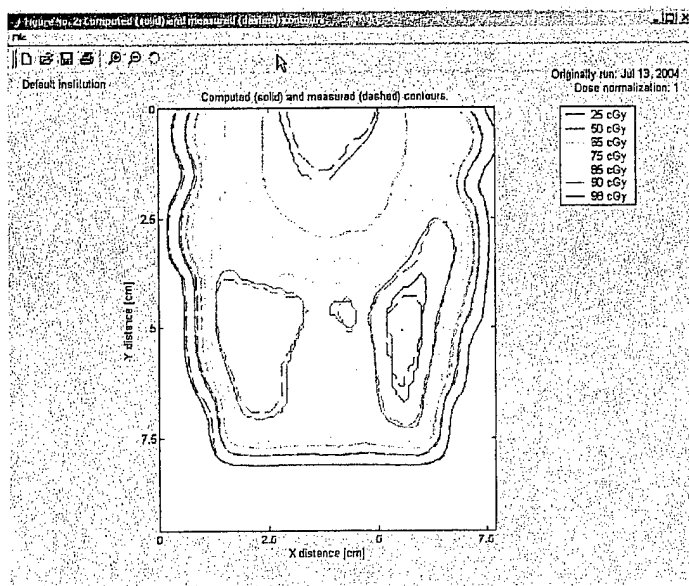
2. COMPARISON OF CALCULATED DELIVERABLE DATA

Figure 46 represents a vertical dose profile comparison of the calculated deliverable data using the ADAC model versus the Jaw model.

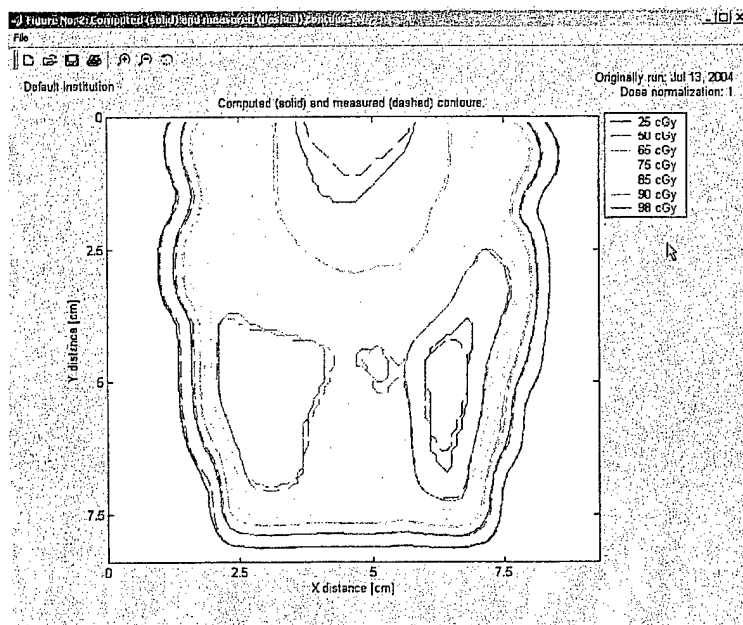




All profile comparisons between the models agree well.



There is some difference noted between the two maps at the 85cGy and higher isodose lines.

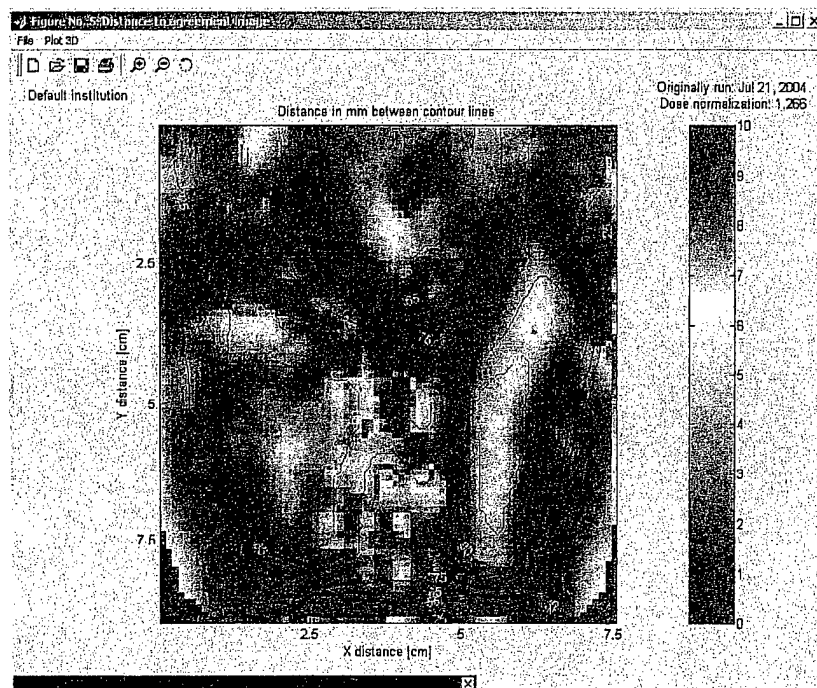
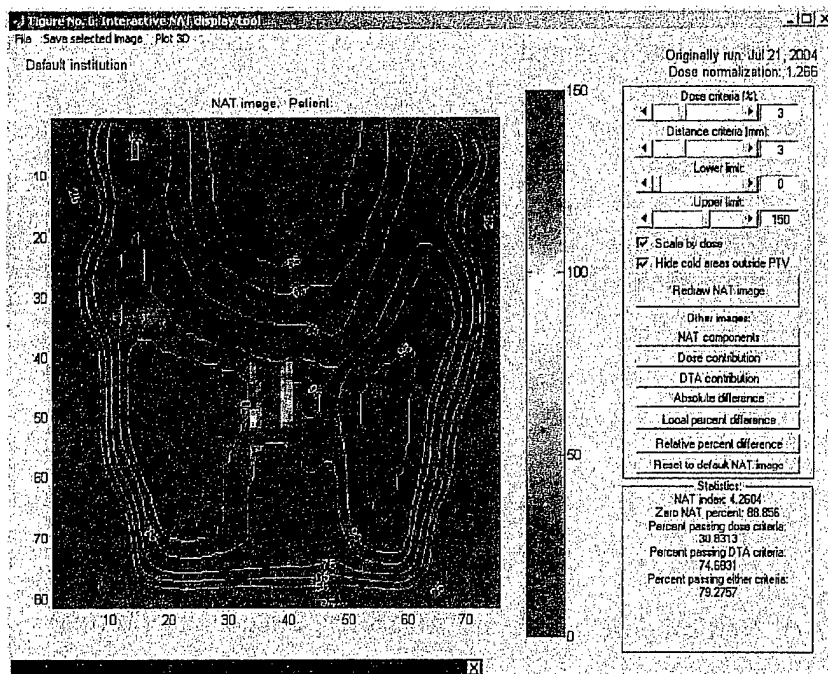


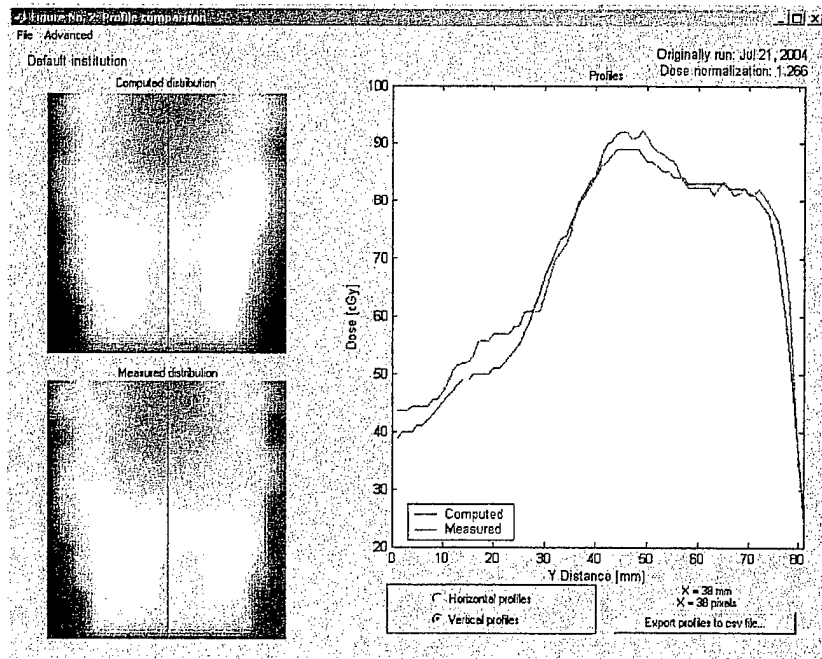
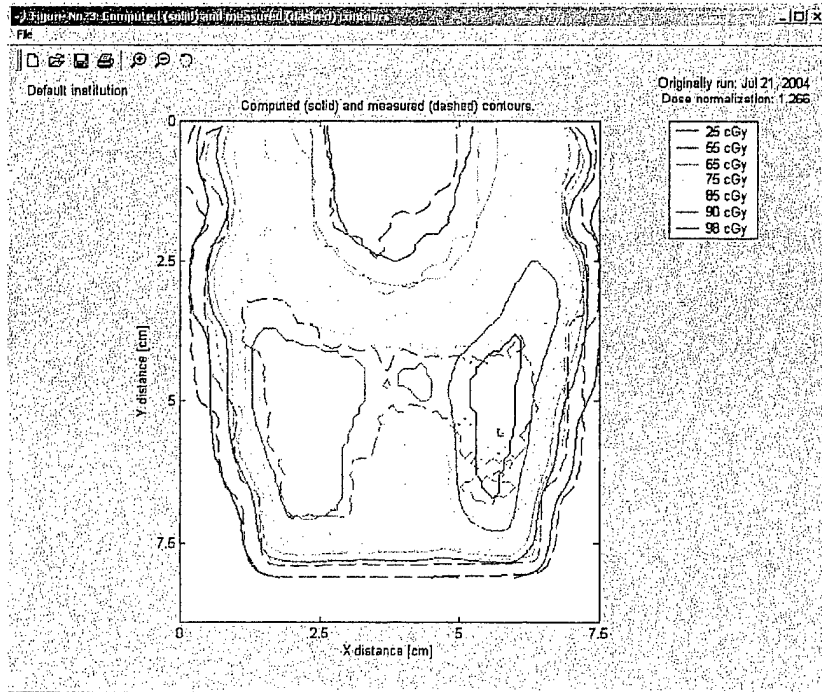
There is some difference noted between the two maps at the 85cGy and higher isodose lines.

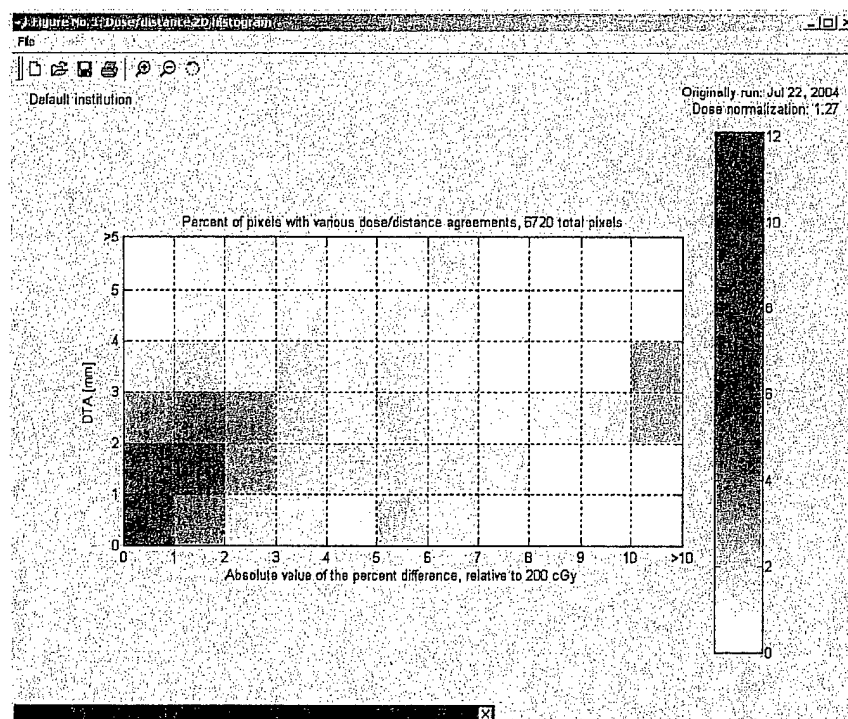
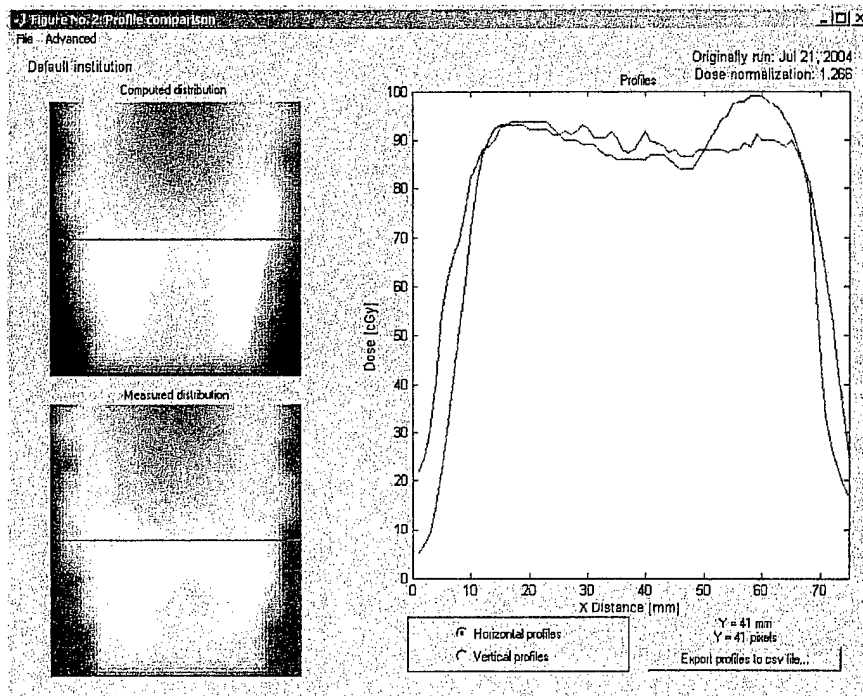
3. COMPARISON OF CALCULATED DELIVERABLE VS. DELIVERABLE MEASURED DATA

To determine which model best predicted its' measured dose the calculated deliverable data was compared to the deliverable measured data for each model. The following figures represent this series of comparisons. All compare the same prostate posterior to anterior IMRT view.

Figures 52-57 represent various tests used to compare the ADAC calculated deliverable plan versus the deliverable measured data from the ADAC model.

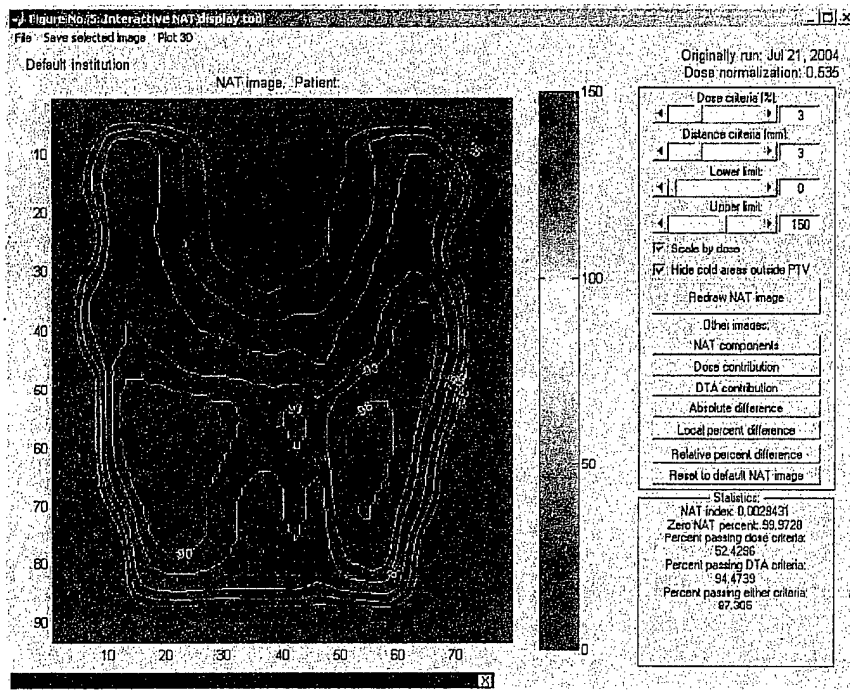


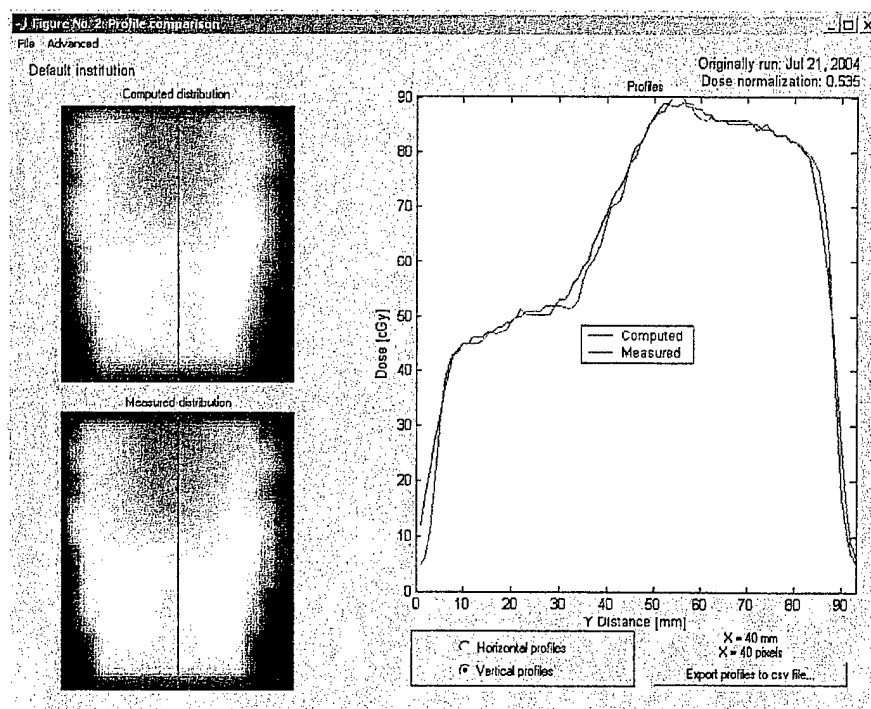
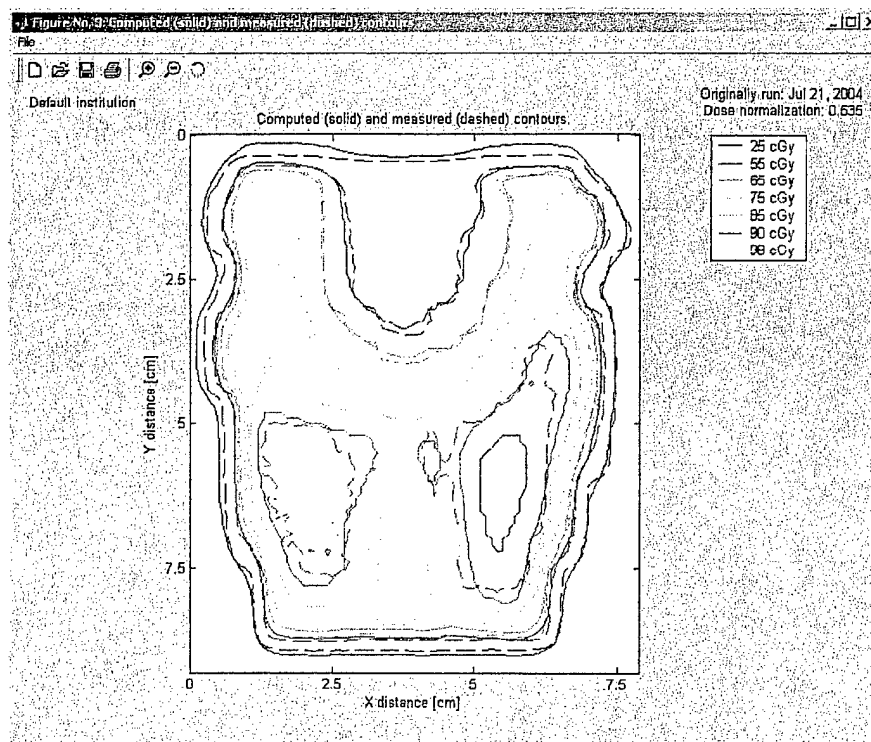


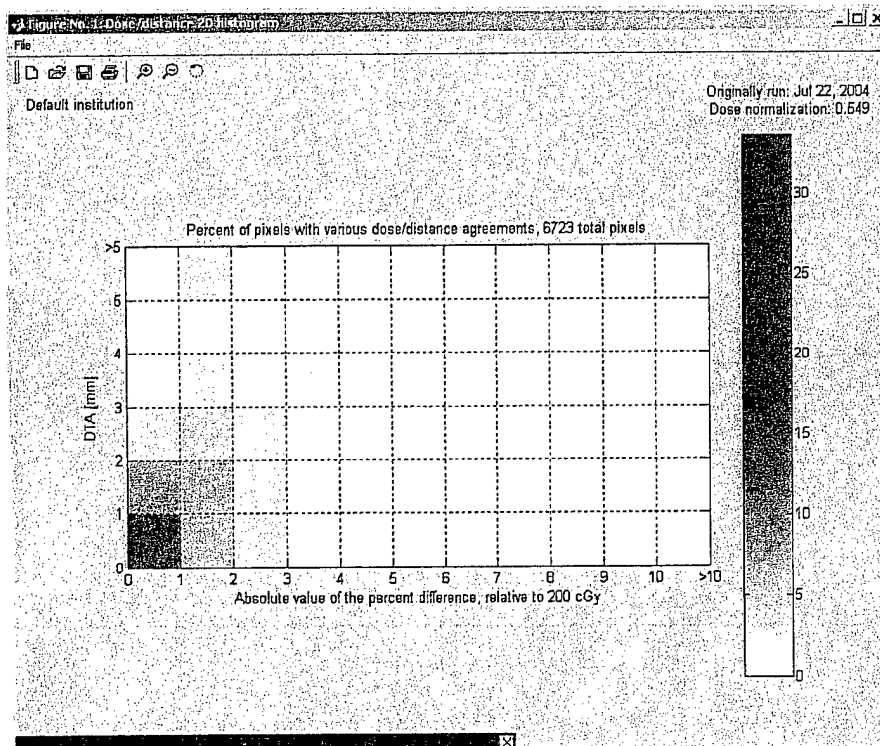
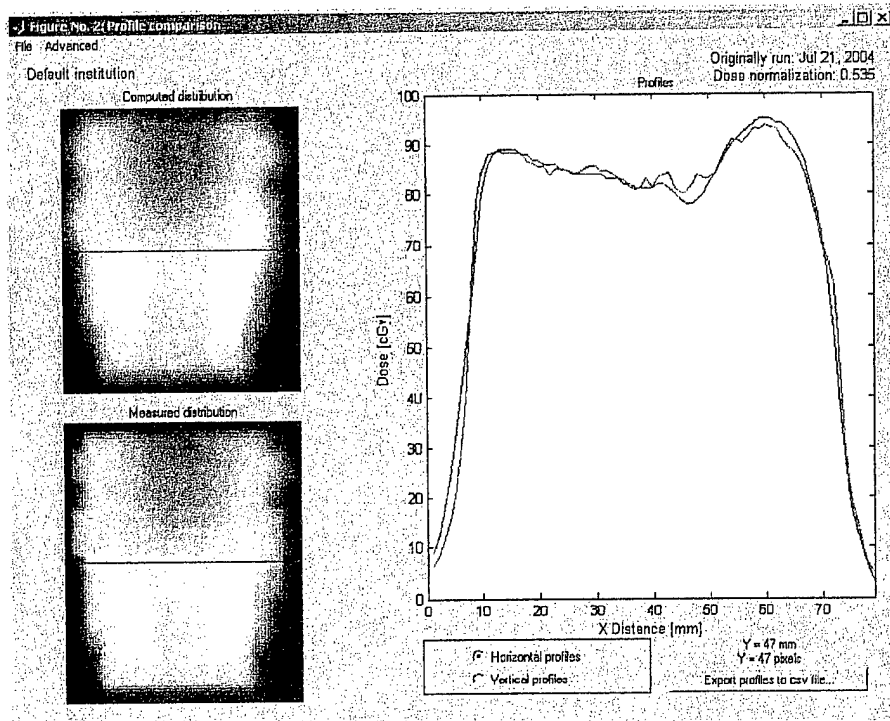


For the prostate plan, the ADAC optimized plan did much better at predicting the measured dose versus the neck plan. The distance to agreement score was 79%. Looking at the 2D histogram, there were some borderline dose discrepancies, which fell outside the distance threshold of 3mm.

Figures 58-63 represent the comparison between the MLC model calculated deliverable dose versus the deliverable measured dose.

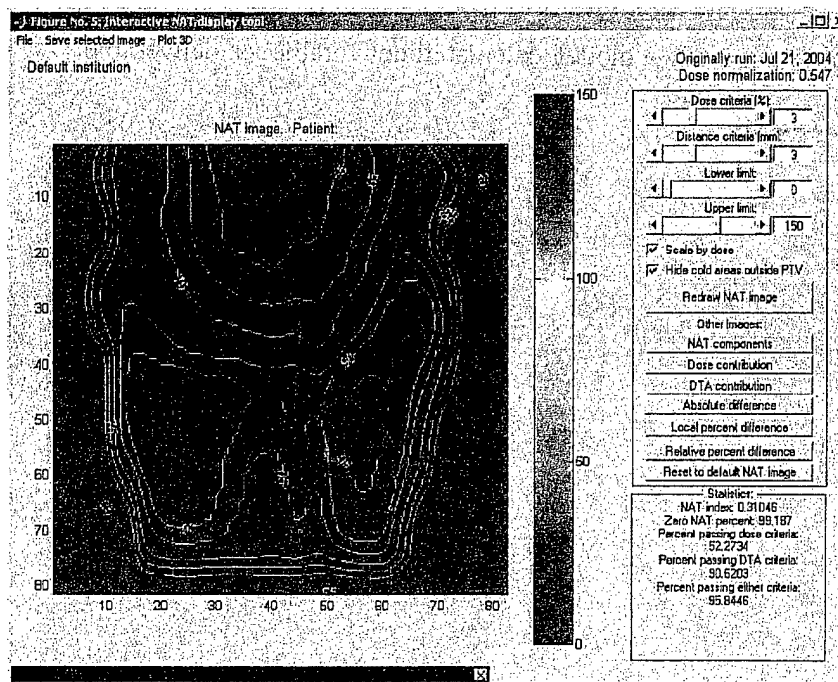


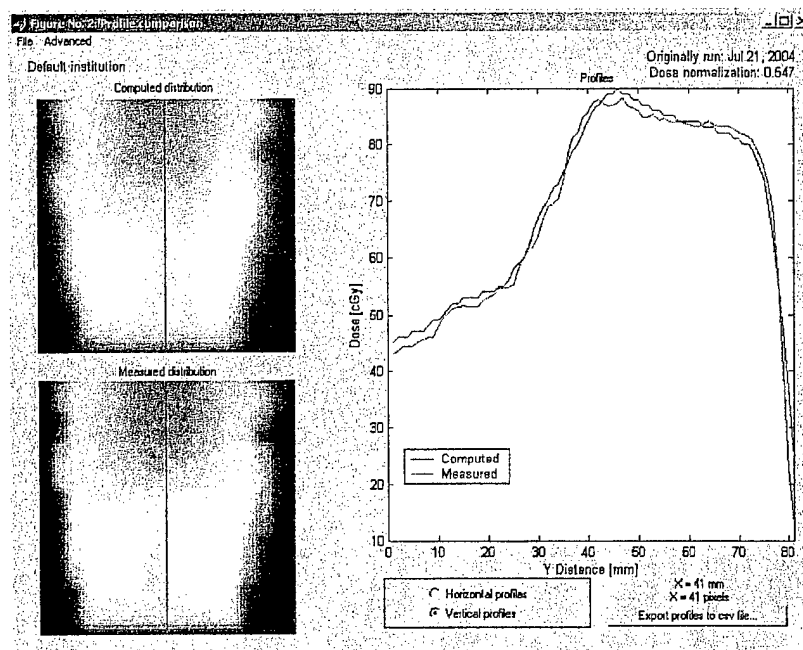
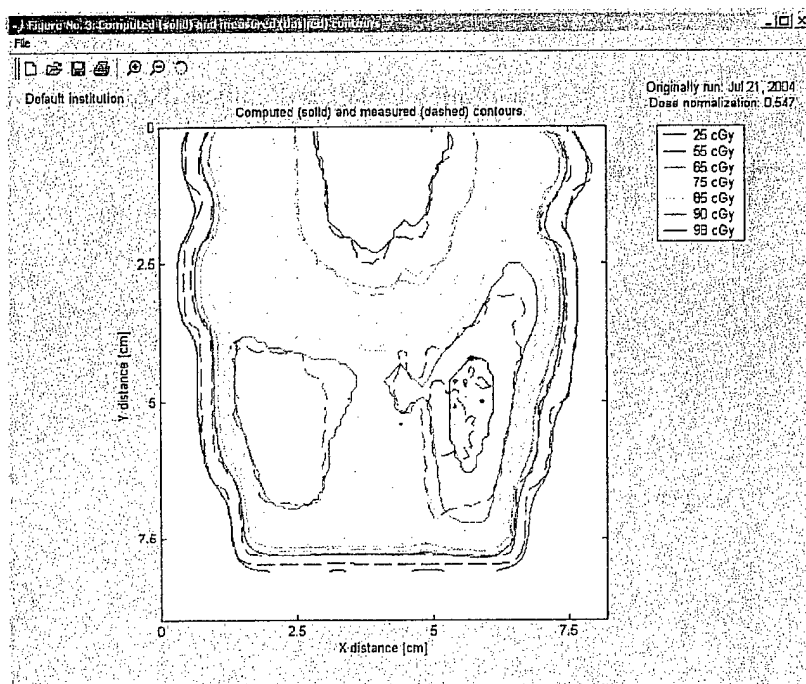


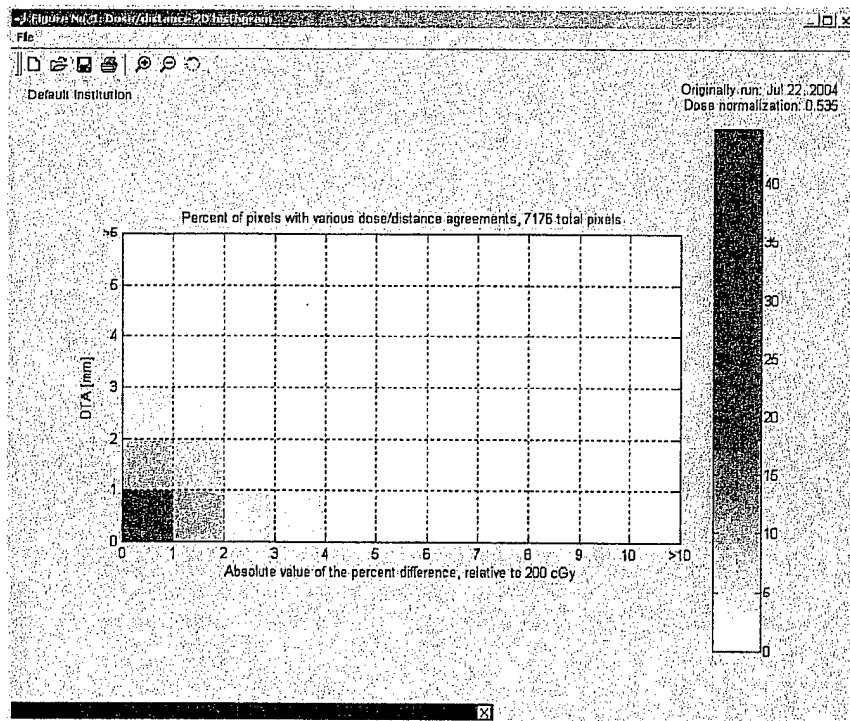
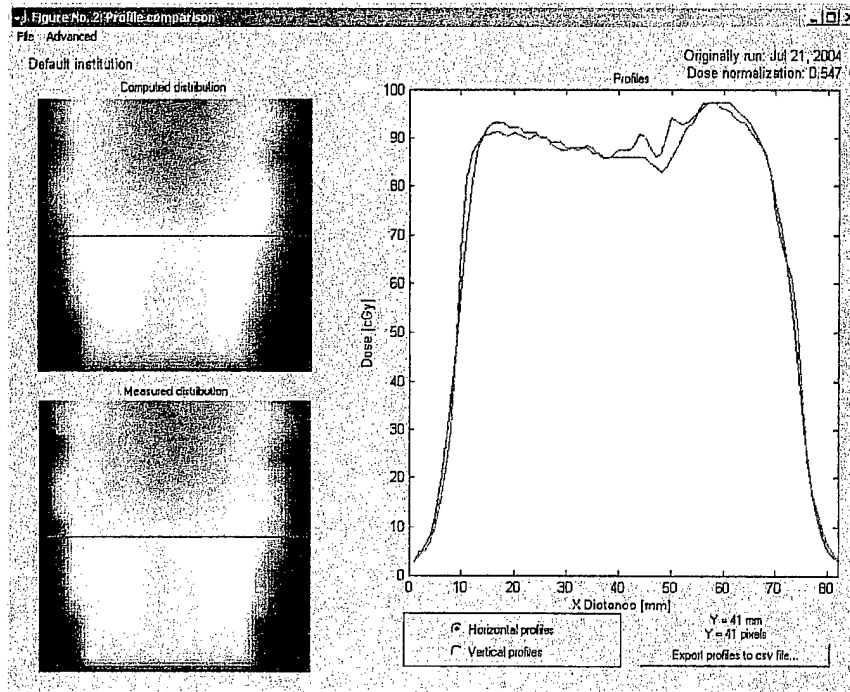


The high distance to agreement score of 97% for this comparison suggests that the MLC model was a very accurate predictor for measured dose. This is significantly higher than the ADAC model scored.

Figures 64-69 represent the comparison between the Jaw planar dose data and the Jaw measured dose data.







The Jaw model had a distance to agreement score slightly less than the MLC model but still predicted measured dose from its own plan very well. This was also significantly higher than the ADAC model scored. The following summarizes the NAT and DTA scores.

Calculated deliverable vs. deliverable measured from film

	NAT Index	Zero NAT %	% passing NAT criteria	% passing DTA criteria	% passing either criteria
ADAC Model	4.26	88.86	30.83	74.68	79.28
MLC Model	0	99.97	52.43	94.47	97.31
Jaw Model	0.31	99.19	52.27	90.62	95.84

IV. DISCUSSION

Historically, treatment planning systems do not include beam data for field sizes less than $3\text{cm} \times 3\text{cm}$ in the beam model because it is rare to plan with such small fields. However, in IMRT, major portions of the treatment can be given with fields as small as $1\text{cm} \times 1\text{cm}$. These small field sizes and their inherent dosimetric peculiarities are relatively new to treatment planning algorithms and have to be carefully addressed in the beam model in order to get accurate dose calculations for IMRT.

The method described in this report was a method used at our institution to test the ADAC Pinnacle³ Model (ADAC), a model which we implemented based on large field dosimetry, against two other models (MLC and Jaw), based on small field dosimetry.

When comparing the beam profiles, there were differences noted between the three models that ranged from 2% - 20%. This was especially prominent for the smaller field sizes, i.e., $1\text{cm}^2 - 3\text{cm}^2$.

Using a Normalized Agreement Test and a Distance to Agreement Test, we were able to determine that the small field models were better predictors for delivered dose. Although it is ultimately up to the physicist and oncologist to determine what dose and distance thresholds are acceptable, by convention a 3% dose or 3mm variance are considered the norm.^{13,14} The Normalized Agreement Test and Distance to Agreement scores were, on average, 24% higher for the Jaw and MLC models versus the ADAC model. These results were expected since the ADAC model does not include dosimetry

data for small field sizes. The fact that the Jaw model scored almost as well as the MLC model suggests that it is the small field modeling itself that contributes to the overall dose and distance agreement and that an MLC model versus a Jaw model provides only a slightly better performance.

All three models scored lower for the head and neck plan versus the prostate plan. This is likely a function of the increased modulation for this particular plan. The fact that there was a greater difference in scores with the head and neck plan versus the prostate plan, (30% difference for the head and neck plan and 17% difference for the prostate plan), suggests that with a plan that has increased modulation, the beam modeling becomes even more critical.

Based on our results, we suggest that treatment planning system users evaluate the performance of their beam models and consider whether to incorporate small field data into the model. This is especially warranted with IMRT plans that have extensive modulation. Due to the increased numbers of small field sizes generated by IMRT plans, the treatment planning system will need small field dosimetric data to accurately predict dose.

IV. CONCLUSIONS

The objective of this work was to test whether ADAC Pinnacle³ IMRT treatment planning software can accurately predict doses for small field sizes. It was our hypothesis that the ADAC model would not accurately predict dose for small fields. It was further hypothesized that this inaccuracy would be clinically significant. Our results show that small field models, using small field dosimetry data from either jaw or MLC collimation, were better predictors for IMRT dose than the ADAC Pinnacle³ model.

The data suggest that a clinically significant difference can arise between IMRT plans that are based on large and small field models. Further studies would be required to determine whether or not patient outcome would be affected by the choice of the beam sizes used to model the radiation characteristics.

APPENDIX

The ADAC Pinnacle3 Collapsed Cone Convolution

Superposition Dose Model

Todd McNutt, Ph.D. – Director of Product Development

ADAC's Pinnacle3 3D treatment planning system uses a Collapsed Cone Convolution Superposition computation to determine the dose distribution in patients from external photon beams. The Pinnacle3 Convolution Superposition dose model is a true three dimensional dose computation which intrinsically handles the effects of patient heterogeneities on both primary and secondary scattered radiation. This computation method is uniquely able to account for dose distributions in areas where the electronic equilibrium is perturbed, such as tissue-air interfaces and tissue-bone interfaces. While other convolution techniques account for the effects of patient heterogeneities on primary radiation, they neglect the effects of heterogeneities on scattered radiation in the final dose distribution. In addition, the nature of the Convolution Superposition dose model makes it ideally suited to handle optimization and intensity modulated radiation therapy planning.

The Convolution Superposition Dose Model

The Pinnacle3 Convolution Superposition dose algorithm is based on the work of Mackie, et al. Rather than correcting measured dose distributions, the Convolution Superposition algorithm computes dose distributions from first principles and, therefore, can account for the effects of beam modifiers, the external patient contour, and tissue heterogeneities on the dose distribution.

The Convolution Superposition dose model consists of four parts:

- Modeling the incident energy fluence as it exits the accelerator head.
- Projection of this energy fluence through the density representation of a patient to compute a TERMA (Total Energy Released per unit Mass) volume.
- A three-dimensional superposition of the TERMA with an energy deposition kernel using a ray-tracing technique to incorporate the effects of heterogeneities on lateral scatter.
- Electron contamination is modeled with an exponential falloff which is added to the dose distribution after the photon dose is computed.

The following sections describe each part of the model in more detail.

Modeling the Incident Energy Fluence as it exits the Accelerator

The incident energy fluence distribution is modeled as a two-dimensional array which describes the radiation exiting the head of the linear accelerator. The parameters defining this array is defined during physics data modeling. The starting point for photon modeling is a uniform plane of energy fluence describing the intensity of the radiation exiting the accelerator head. The fluence model is then adjusted to account for the flattening filter, the accelerator head, and beam modifiers such as blocks, wedges and compensators.

- The “horns” in the beam produced by the flattening filter are modeled by removing an inverted cone from the distribution.
- Off-focus scatter produced in the accelerator head is modeled by defining a 2D Gaussian function as a scatter source and adjusting the incident energy fluence based on the portion of the Gaussian distribution visible from each point in the incident energy

fluence plane.

- The geometric penumbra is modeled by convolving the array with a focal spot blurring function.
- During planning, the shape of the field produced by blocks or multi-leaf collimators is cut out of the array leaving behind the corresponding transmission through the shape-defining entity.
- Beam modifiers such as wedges and compensators are included in the array by attenuating the energy fluence by the corresponding thickness of the modifier. For static wedges and compensators, a radiological depth array is also stored which allows for proper modeling of the beam hardening due to the presence of the beam modifiers during the projection of the incident fluence array.

Dynamic beam delivery with intensity-modulation or dynamic wedges is easily handled using the incident energy fluence array. For these beams, the radiological depth array is not needed to account for beam hardening.

Projection of Energy Fluence through a CT Patient Representation

The incident energy fluence plane is projected through the CT patient representation and attenuated using mass attenuation coefficients. These coefficients are stored in a three-dimensional lookup table as a function of density, radiological depth, and off-axis angle. Patient heterogeneities are taken into account with the density dependence. Beam hardening through the patient is accounted for with the radiological depth dependence, and the off-axis softening of the energy spectrum is produced with the off-axis angle dependence. To account for the changes in the photon energy spectrum at different locations in the beam, the mass attenuation coefficient lookup table is produced using

a weighted sum of several mono-energetic tables. The TERMA (Total Energy Released per unit Mass) volume is computed by projecting the incident energy fluence through the patient density volume using a ray-tracing technique. A given ray's direction is determined based on the position of the radiation source and the particular location in the incident fluence plane. At each voxel in the ray path, the TERMA is computed using the attenuated energy fluence along the ray and the mass attenuation coefficient at the particular density, radiological depth, and off-axis angle.

3D Superposition of an Energy Deposition Kernel

The three-dimensional dose distribution in the patient is computed by superposition of the TERMA volume with the energy deposition kernel. The kernel represents the spread of energy from the primary photon interaction site throughout the associated volume. Poly-energetic kernels are produced by combining a series of Monte Carlo-generated mono-energetic energy deposition kernels. The superposition is carried out using a ray tracing technique similar to that used in the projection of the incident energy fluence. The kernel is inverted so that the dose can be computed in only a portion of the patient (TERMA) volume if desired. This allows for point dose computation and decreases computation time. The rays from the dose deposition site are cast in three dimensions. At each voxel of the TERMA traversed along a ray, the contribution of dose to the dose deposition site is computed and accumulated using the TERMA and the kernel value at the current radiological distance. Using the radiological distance along the ray also allows the kernel to be scaled to account for the presence of heterogeneities with respect to scattered radiation in all directions. The dose computation described above determines the dose from a single beam. Multiple beams are computed independently and the entire

3D dose distribution is created by adding the dose from each beam together according to the corresponding beam weight.

Adaptive Convolution Superposition

An Adaptive Convolution Superposition approach has also been implemented in Pinnacle3. This uses the calculation technique described above with some slight modifications. The speed of the computation is increased by adaptively varying the resolution of the dose computation grid depending on the curvature of the TERMA and dose distribution. First, the dose in a coarse 3D grid is computed and then the curvature in the TERMA distribution is assessed. In regions where the curvature is high, the dose is computed at intermediate points to provide higher resolution. The system adaptively increases the resolution in regions of high curvature until an acceptable resolution is used. In regions of low curvature, the dose is interpolated from the coarse dose grid. This technique decreases the computation time by a factor of 2-3 without compromising the accuracy of the Convolution Superposition calculation in the presence of heterogeneities.

Other Model-Based Algorithms

Other model-based algorithms, including 3D Fast Fourier Transform (FFT) techniques and differential pencil beam models which use FFTs on two-dimensional planes, use a projection of the incident energy fluence similar to that used in Pinnacle3 to determine the TERMA volume. They differ in that they do not use the superposition technique in the convolution process. The FFT techniques require the assumption of an invariant kernel, which inherently assumes a homogeneous density representation during the

convolution process. This technique reduces the accuracy of the computation because it ignores the effects of heterogeneities on laterally scattered radiation. Some post computation corrections may be performed to help alleviate the error. In contrast, by scaling the rays from the primary dose deposition site, the Convolution Superposition method accurately and intrinsically models the effects of lateral scatter from tissue heterogeneities, a requirement for calculating dose from conformal and intensity modulated fields.

ADAC Laboratories
540 Alder Dr.
Milpitas, CA 95035
Tel: (408)321-9100 (800)538-8531
Fax: (408)577-0907 www.adaclabs.com
MBA-X0010, Rev. B

Although the FFT algorithms have a fast computation speed per computation point, they require full computation of dose over the entire TERMA volume. For irregular field calculations, point doses, plane doses, or other situations where the planner is only interested in the dose to smaller regions, the FFT algorithms still require the dose to be computed over the entire volume. The Convolution Superposition method can accurately compute the dose to a single point with the inverted energy deposition kernel. Therefore, depending on the planning situation, the desired dose calculation may be faster using the Convolution Superposition calculation than when using the FFT calculation.

The ability to define a smaller calculation matrix also results in a calculation speed advantage with the Convolution Superposition model for inverse planning and optimization of intensity modulated beams where computation of dose need only be performed in limited regions during the optimization process.

LITERATURE CITED

- 1 Y. Xiao, J. Galvin, et al., Medical Physics 27 (9), 2093 (2000)
- 2 J.E. Bayouth, S.M. Morrill, Medical Physics 30 (9), 2545 (2003)
- 3 W.U. Laub, T.Wong, Medical Physics 30 (3), 341 (2003)
- 4 J.E. Bayouth, S.M. Morrill, Medical Physics 30 (9), 2545 (2003)
- 5 J.R. Palta, D.K. Yueng, et. al., Medical Physics 23, 1219 (1996)
- 6 M.S. Huq, Y. Yu, et. al., Medical Physics 22, 241 (1995)
- 7 M.Stasi, B. Biaotto, et. al., Radiology Medicine 101, 187 (1999)
- 8 Varian Medical Systems, Treatment Delivery, Multi-leaf Collimators,
"Description of Multi-leaf Collimators"
- 9 P. Hanny et al., "Radiographic Film Calibration Using High Density
Material", UTHSCSA (2004)
- 10 X.R. Zhu, P.A. Jursinic, D.F. Grimm et al., Medical Physics. 29 (10) 2438
(2002)
- 11 T.R. Mackie, J.W. Scrimger, J.J. Battista, "A convolution method of
calculating dose for 15-MV x-rays", Medical Physics 12, 188-196 (1985)
- 12 T. McNutt, "The ADAC Pinnacle3 Collapsed Cone Convolution
Superposition Dose Model", Phillips Medical Systems, Training and
Education ROS, White Papers
- 13 Arthur J. Olch, Medical Physics 29, 2484 (2002)
- 14 Peter Björk, Tommy Knöös, Per Nilsson, Medical Physics 27, 2580 (2000)